The Present Status, Challenges, and Future Developments in Computational Fluid Dynamics

Antony Jameson
Department of Mechanical and Aerospace Engineering
Princeton University
Princeton, New Jersey 08544 USA

1 SUMMARY

This paper presents a perspective on computational fluid dynamics as a tool for aircraft design. It addresses the requirements for effective industrial use, and trade-offs between modelling accuracy and computational costs. Issues in algorithm design are discussed in detail, together with a unified approach to the design of shock capturing algorithms. Finally, the paper discusses the use of techniques drawn from control theory to determine optimal aerodynamic shapes. In the future multidisciplinary analysis and optimization should be combined to provide an integrated numerical design environment.

2 INTRODUCTION

Computational methods first began to have a significant impact on aerodynamics analysis and design in the period of 1965-75. This decade saw the introduction of panel methods which could solve the linear flow models for arbitrarily complex geometry in both subsonic and supersonic flow [58, 147, 178]. It also saw the appearance of the first satisfactory methods for treating the nonlinear equations of transonic flow [123, 122, 63, 64, 43, 54], and the development of the hodograph method for the design of shock free supercritical airfoils [15].

Computational Fluid Dynamics (CFD) has now matured to the point at which it is widely accepted as a key tool for aerodynamic design. Algorithms have been the subject of intensive development for the past two decades. The principles underlying the design and implementation of robust schemes which can accurately resolve shock waves and contact discontinuities in compressible flows are now quite well established. It is also quite well understood how to design high order schemes for viscous flow, including compact schemes and spectral methods. Adaptive refinement of the mesh interval (h) and the order of approximations (p) has been successfully exploited both separately and in combination in the h-p method [126]. A continuing obstacle to the treatment of configurations with complex geometry has been the problem of mesh generation. Several general techniques have been developed, including algebraic transformations and methods based on the solution of elliptic and hyperbolic equations. In the last few years methods using unstructured meshes have also begun to gain more general acceptance. The Dassault-INRIA group led the way in developing a finite element method for transonic potential flow. They obtained a solution for a complete Falcon 50 as early as 1982 [25]. Euler methods for unstructured meshes have been the subject of intensive development by several groups since 1985 [110, 82, 81, 163, 14], and Navier-Stokes methods on unstructured meshes have also been demonstrated [117, 118, 11].

Despite the advances that have been made, CFD is still not being exploited as effectively as one would like in the design process. This is partly due to the long set-up and high costs, both human and computational of complex flow simulations. The essential requirements for industrial use are:

1. assured accuracy
2. acceptable computational and human costs
3. fast turn around.

Improvements are still needed in all three areas. In particular, the fidelity of modelling of high Reynolds number viscous flows continues to be limited by computational costs. Consequently accurate and cost effective simulation of viscous flow at Reynolds numbers associated with full scale flight, such as the prediction of high lift devices, remains a challenge. Several routes are available toward the reduction of computational costs, including the reduction of mesh requirements by the use of higher order schemes, im-

proved convergence to a steady state by sophisticated acceleration methods, fast inversion methods for implicit schemes, and the exploitation of massively parallel computers.

Another factor limiting the effective use of CFD is the lack of good interfaces to computer aided design (CAD) systems. The geometry models provided by existing CAD systems often fail to meet the requirements of continuity and smoothness needed for flow simulation, with the consequence that they must be modified before they can be used to provide the input for mesh generation. This bottleneck, which impedes the automation of the mesh generation process, needs to be eliminated, and the CFD software should be fully integrated in a numerical design environment. In addition to more accurate and cost-effective flow prediction methods, better optimizations methods are also needed, so that not only can designs be rapidly evaluated, but directions of improvement can be identified. Possession of techniques which result in a faster design cycle gives a crucial advantage in a competitive environment.

A critical issue, examined in the next section, is the choice of mathematical models. What level of complexity is needed to provide sufficient accuracy for aerodynamic design, and what is the impact on cost and turn-around time? Section 3 addresses the design of numerical algorithms for flow simulation. Section 4 presents the results of some numerical calculations which require moderate computer resources and could be completed with the fast turn-around required by industrial users. Section 5 discusses automatic design procedures which can be used to produce optimum aerodynamic designs. Finally, Section 7 offers an outlook for the future.

3 THE COMPLEXITY OF FLUID FLOW AND MATHEMATICAL MODELLING

3.1 The Hierarchy of Mathematical Models

Many critical phenomena of fluid flow, such as shock waves and turbulence, are essentially nonlinear. They also exhibit extreme disparities of scales. While the actual thickness of a shock wave is of the order of a mean free path of the gas particles, on a macroscopic scale its thickness is essentially zero. In turbulent flow energy is transferred from large scale motions to progressively smaller eddies until the scale becomes so small that the motion is dissipated by viscosity. The ratio of the length scale of the global flow to that of the smallest persisting eddies is of the order $\mathrm{Re}^{\frac{3}{4}}$, where Re is the Reynolds number, typically in the range of 30 million for an aircraft. In order to resolve such scales in all three space directions a computational grid with the order of $\mathrm{Re}^{\frac{9}{4}}$ cells would be required. This is beyond the range of any current or foreseeable computer. Consequently mathematical models with varying degrees of simplification have to be introduced in order to make computational simulation of flow feasible and produce viable and cost-effective methods.

Figure 1 (supplied by Pradeep Raj) indicates a hierarchy of models at different levels of simplification which have proved useful in practice. Efficient flight is generally achieved by the use of smooth and streamlined shapes which avoid flow separation and minimize viscous effects, with the consequence that useful predictions can be made using inviscid models. Inviscid calculations with boundary layer corrections can provide quite accurate predictions of lift and drag when the flow remains attached, but iteration between the inviscid outer solution and the inner boundary layer solution becomes increasingly difficult with the onset of separation. Procedures for solving the full viscous equations are likely to be needed for the simulation of arbitrary complex separated flows, which may occur at high angles of attack or with bluff bodies. In order to treat flows at high Reynolds numbers, one is generally forced to estimate turbulent effects by Reynolds averaging of the fluctuating components. This requires the introduction of a turbulence model. As the available computing power increases one may also aspire to large eddy simulation (LES) in which the larger scale eddies are directly calculated, while the influence of turbulence at scales smaller than the mesh interval is represented by a subgrid scale model.

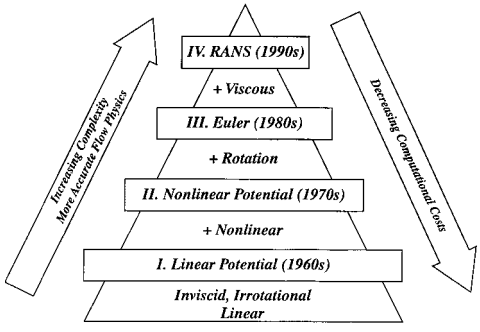

Figure 1: Hierarchy of Fluid Flow Models

3.2 Computational Costs

Computational costs vary drastically with the choice of mathematical model. Panel methods can be effectively used to solve the linear potential flow equation with higher-end personal computers (with an Intel 80486 microprocessor, for example). Studies of the dependency of the result on mesh refinement, performed by this author and others, have demonstrated that inviscid transonic potential flow or Euler solutions for an airfoil can be accurately calculated on a mesh with 160 cells around the section, and 32 cells normal to the section. Using multigrid techniques 10 to 25 cycles are enough to obtain a converged result. Consequently airfoil calculations can be performed in seconds on a Cray YMP, and can also be performed on 486-class personal computers. Correspondingly accurate three-dimensional inviscid calculations can be performed for a wing on a mesh, say with $192\times32\times48 = 294,912$ cells, in about 5 minutes on a single processor Cray YMP, or less than a minute with eight processors, or in 1 or 2 hours on a workstation such as a Hewlett Packard 735 or an IBM 560 model.

Viscous simulations at high Reynolds numbers require vastly greater resources. Careful two-dimensional studies of mesh requirements have been carried out at Princeton by Martinelli [114]. He found that on the order of 32 mesh intervals were needed to resolve a turbulent boundary layer, in addition to 32 intervals between the boundary layer and the far field, leading to a total of 64 intervals. In order to prevent degradations in accuracy and convergence due to excessively large aspect ratios (in excess of 1,000) in the surface mesh cells, the chordwise resolution must also be increased to 512 intervals. Reasonably accurate solutions can be obtained in a 512×64 mesh in 100 multigrid cycles. Translated to three dimensions, this would imply the need for meshes with 5–10 million cells (for example, $512\times64\times256 = 8{,}388{,}608$ cells as shown in Figure 2). When simulations are performed on less fine meshes with, say, 500,000 to 1 million cells, it is very hard to avoid mesh dependency in the solutions as well as sensitivity to the turbulence model.

A typical algorithm requires of the order of 5,000 floating point operations per mesh point in one multigrid iteration. With 10 million mesh points, the operation count is of the order of 0.5×10^{11} per cycle. Given a computer capable of sustaining 10^{11} operations per second (100 gigaflops), 200 cycles could then be performed in 100 seconds. Simulations of unsteady viscous flows (flutter, buffet) would be likely to require 1,000–10,000 time steps. A further progression to large eddy simulation of complex configurations would require even greater resources. The following estimate is due to W.H. Jou [90]. Suppose that a conservative estimate of the size of eddies in a boundary layer that ought to be resolved is 1/5 of the boundary layer thickness. Assuming that 10 points are needed to resolve a single eddy, the mesh interval should then be 1/50 of the boundary layer thickness. Moreover, since the eddies are three-dimensional, the same mesh interval should be used in all three directions. Now, if the boundary layer thickness is of the order of 0.01 of the chord length, 5,000 intervals will be needed in the chordwise direction, and for a wing with an aspect ratio of 10, 50,000 intervals will be needed in the spanwise direction. Thus, of the order of $50\times5,000\times50,000$ or 12.5 billion mesh points would be needed in the boundary layer. If the time dependent behavior of the eddies is to be fully resolved using time steps on the order of the time for a wave to pass through a mesh interval, and one allows for a total time equal to the time required for waves to travel three times the length of the chord, of the order of 15,000 time steps would be needed. Performance beyond the teraflop (10^{12} operations per second) will be needed to attempt calculations of this nature, which also have an information content far beyond what is needed for enginering analysis and design. The designer does not need to know the details of the eddies in the boundary layer. The primary purpose of such calculations is to improve the calculation of averaged quantities such as skin friction, and the prediction of global behavior such as the onset of separation. The main current use of Navier-Stokes and large eddy simulations is to try to gain an improved insight into the physics of turbulent flow, which may in turn lead to the development of more comprehensive and reliable

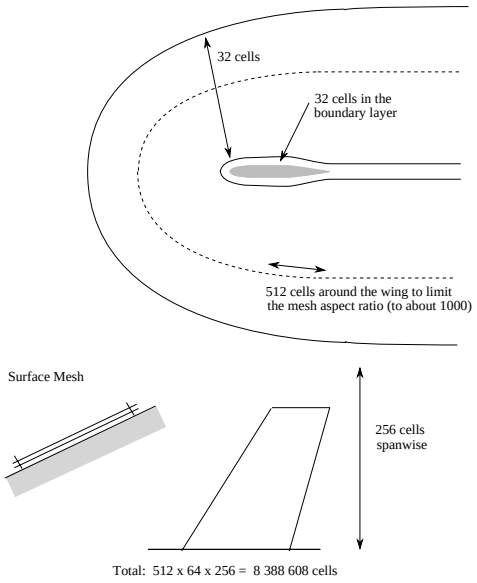

Figure 2: Mesh Requirements for a Viscous Simulation

turbulence models.

3.3 Turbulence Modelling

It is doubtful whether a universally valid turbulence model, capable of describing all complex flows, could be devised [52]. Algebraic models [30, 9] have proved fairly satisfactory for the calculation of attached and slightly separated wing flows. These models rely on the boundary layer concept, usually incorporating separate formulas for the inner and outer layers, and they require an estimate of a length scale which depends on the thickness of the boundary layer. The estimation of this quantity by a search for a maximum of the vorticity times a distance to the wall, as in the Baldwin-Lomax model, can lead to ambiguities in internal flows, and also in complex vortical flows over slender bodies and highly swept or delta wings [40, 115]. The Johnson-King model [88], which allows for non-equilibrium effects through the introduction of an ordinary differential equation for the maximum shear stress, has improved the prediction of flows with shock induced separation [148, 91].

Closure models depending on the solution of transport equations are widely accepted for industrial applications. These models eliminate the need to estimate a length scale by detecting the edge of the boundary layer. Eddy viscosity models typically use two equations for the turbulent kinetic energy k and the dissipation rate ϵ, or a pair of equivalent quantities [89, 177, 160, 1, 121, 35]. Models of this type generally tend to present difficulties in the region very close to the wall. They also tend to be badly conditioned for numerical solution. The $k-l$ model [154] is designed to alleviate this problem by taking advantage of the linear behaviour of the length scale l near the wall. In an alternative approach to the design of models which are more amenable to numerical solution, new models requiring the solution of one transport equation have recently been introduced [10, 159]. The performance of the algebraic models remains competitive for wing flows, but the one- and two-equation models show promise for broader classes of flows. In order to achieve greater universality, research is also being pursued on more complex Reynolds stress transport models, which require the solution of a larger number of transport equations.

Another direction of research is the attempt to devise more rational models via renormalization group (RNG) theory [181, 155]. Both algebraic and two-equation $k-\epsilon$ models devised by this approach have shown promising results [116].

The selection of sufficiently accurate mathematical models and a judgment of their cost effectiveness ultimately rests with industry. Aircraft and spacecraft designs normally pass through the three phases of conceptual design, preliminary design, and detailed design. Correspondingly, the appropriate CFD models will vary in complexity. In the conceptual and preliminary design phases, the emphasis will be on relatively simple models which can give results with very rapid turn-around and low computer costs, in order to evaluate alternative configurations and perform quick parametric studies. The detailed design stage requires the most complete simulation that can be achieved with acceptable cost. In the past, the low level of confidence that could be placed on numerical predictions has forced the extensive use of wind tunnel testing at an early stage of the design. This practice was very expensive. The limited number of models that could be fabricated also limited the range of design variations that could be evaluated. It can be anticipated that in the future, the role of wind tunnel testing in the design process will be more one of verification. Experimental research to improve our understanding of the physics of complex flows will continue, however, to play a vital role.

4 CFD ALGORITHMS

4.1 Difficulties of Flow Simulation

The computational simulation of fluid flow presents a number of severe challenges for algorithm design. At the level of inviscid modeling, the inherent nonlinearity of the fluid flow equations leads to the formation of singularities such as shock waves and contact discontinuities. Moreover, the geometric configurations of interest are extremely complex, and generally contain sharp edges which lead to the shedding of vortex sheets. Extreme gradients near stagnation points or wing tips may also lead to numerical errors that can have global influence. Numerically generated entropy may be convected from the leading edge for example, causing the formation of a numerically induced boundary layer which can lead to separation. The need to treat exterior domains of infinite extent is also a source of difficulty. Boundary conditions imposed at artificial outer boundaries may cause reflected waves which significantly interfere with the flow. When viscous effects are also included in the simulation, the extreme difference of the scales in the viscous boundary layer and the outer flow, which is essentially inviscid, is another source of difficulty, forcing the use of meshes with extreme variations in mesh interval. For these reasons CFD, has been a driving force for the development of numerical algorithms.

4.2 Structured and Unstructured Meshes

The algorithm designer faces a number of critical decisions. The first choice that must be made is the nature of the mesh used to divide the flow field into discrete subdomains. The discretization procedure must allow for the treatment of complex configurations. The principal alternatives are Cartesian meshes, body-fitted curvilinear meshes, and unstructured tetrahedral meshes. Each of these approaches has advantages which have led to their use. The Cartesian mesh minimizes the complexity of the algorithm at interior points and facilitates the use of high order discretization procedures, at the expense of greater complexity, and possibly a loss of accuracy, in the treatment of boundary conditions at curved surfaces. This difficulty may be alleviated by using mesh refinement procedures near the surface. With their aid, schemes which use Cartesian meshes have recently been developed to treat very complex configurations [120, 149, 22, 94].

Body-fitted meshes have been widely used and are particularly well suited to the treatment of viscous flow because they readily allow the mesh to be compressed near the body surface. With this approach, the problem of mesh generation itself has proved to be a major pacing item. The most commonly used procedures are algebraic transformations [7, 44, 46, 156], methods based on the solution of elliptic equations, pioneered by Thompson [169, 170, 157, 158], and methods based on the solution of hyperbolic equations marching out from the body [161]. In order to treat very complex configurations it generally proves expedient to use a multiblock [176, 150] procedure, with separately generated meshes in each block, which may then be patched at block faces, or allowed to overlap, as in the Chimera scheme [19, 20]. While a number of interactive software systems for grid generation have been developed, such as EAGLE, GRIDGEN, and ICEM, the generation of a satisfactory grid for a very complex configuration may require months of effort.

The alternative is to use an unstructured mesh in which the domain is subdivided into tetrahedra. This in turn requires the development of solution algorithms capable of yielding the required accuracy on unstructured meshes. This approach has been gaining acceptance, as it is becoming apparent that it can lead to a speed-up and reduction in the cost of mesh generation that more than offsets the increased complexity and cost of the flow simulations. Two competing procedures for generating triangulations which have both proved successful are Delaunay triangulation [41, 11], based on concepts introduced at the beginning of the century by Voronoi [174], and the moving front method [111].

4.3 Finite Difference, Finite Volume, and Finite Element Schemes

Associated with choice of mesh type is the formulation of the discretization procedure for the equations of fluid flow, which can be expressed as differential conservation laws. In the Cartesian tensor notation, let x_i be the coordinates, p, ρ, T, and E the pressure, density, temperature, and total energy, and u_i the velocity components. Using the convention that summation over $j = 1, 2, 3$ is implied by a repeated subscript j, each conservation equation has the form

$$\frac{\partial w}{\partial t} + \frac{\partial f_j}{\partial x_j} = 0. \tag{1}$$

For the mass equation

$$w = \rho, \;\; f_j = \rho u_j.$$

For the i momentum equation

$$w_i = \rho u_i, \;\; f_{ij} = \rho u_i u_j + p\delta_{ij} - \sigma_{ij},$$

where σ_{ij} is the viscous stress tensor. For the energy equation

$$w = \rho E, \;\; f_j = (\rho E + p)u_j - \sigma_{jk}u_k - \kappa\frac{\partial T}{\partial x_j},$$

where κ is the coefficient of heat conduction. The pressure is related to the density and energy by the equation of state

$$p = (\gamma - 1)\rho\left(E - \frac{1}{2}u_i u_i\right) \tag{2}$$

in which γ is the ratio of specific heats. In the Navier-Stokes equations the viscous stresses are assumed to be linearly proportional to the rate of strain, or

$$\sigma_{ij} = \mu\left(\frac{\partial u_i}{\partial x_j} + \frac{\partial u_j}{\partial x_i}\right) + \lambda\delta_{ij}\left(\frac{\partial u_k}{\partial x_k}\right), \tag{3}$$

where μ and λ are the coefficients of viscosity and bulk viscosity, and usually $\lambda = -2\mu/3$.

The finite difference method, which requires the use of a Cartesian or a structured curvilinear mesh, directly approximates the differential operators appearing in these equations. In the finite volume method [112], the discretization is accomplished by dividing the domain of the flow into a large number of small subdomains, and applying the conservation laws in the integral form

$$\frac{\partial}{\partial t}\int_\Omega w dV + \int_{\partial\Omega} \mathbf{f}\cdot d\mathbf{S} = 0.$$

Here $\mathbf{F}$ is the flux appearing in equation (1) and $d\mathbf{S}$ is the directed surface element of the boundary $\partial\Omega$ of the domain Ω. The use of the integral form has the advantage that no assumption of the differentiability of the solutions is implied, with the result that it remains a valid statement for a subdomain containing a shock wave. In general the subdomains could be arbitrary, but it is convenient to use either hexahedral cells in a body conforming curvilinear mesh or tetrahedrons in an unstructured mesh.

Alternative discretization schemes may be obtained by storing flow variables at either the cell centers or the vertices. These variations are illustrated in Figure 3 for the two-dimensional case. With a cell-centered scheme the discrete conservation law takes the form

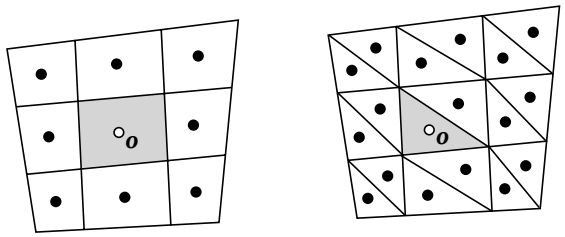

3a: Cell Centered Scheme.

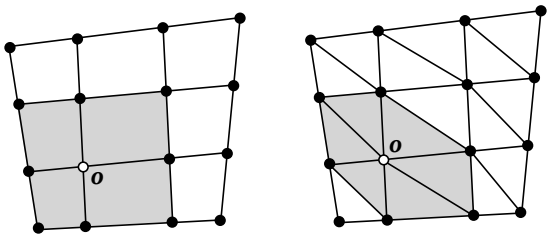

3b: Vertex Scheme.

Figure 3: Structured and Unstructured Discretizations.

$$\frac{d}{dt} wV + \sum_{\text{faces}} \mathbf{f}\cdot\mathbf{S} = 0, \tag{4}$$

where V is the cell volume, and $\mathbf{f}$ is now a numerical estimate of the flux vector through each face. $\mathbf{f}$ may be evaluated from values of the flow variables in the cells separated by each face, using upwind biasing to allow for the directions of wave propagation. With hexahedral cells, equation (4) is very similar to a finite difference scheme in curvilinear coordinates. Under a transformation to curvilinear coordinates ξ_j, equation (1) becomes

$$\frac{\partial}{\partial t}\left(Jw\right) + \frac{\partial}{\partial \xi_i}\left(J\frac{\partial \xi_i}{\partial x_j} f_j\right) = 0, \tag{5}$$

where J is the Jacobian determinant of the transformation matrix $\left[\frac{\partial x_i}{\partial \xi_j}\right]$. The transformed flux $J\frac{\partial \xi_i}{\partial x_j} f_j$ corresponds to the dot product of the flux $\mathbf{f}$ with a vector face area $J\frac{\partial \xi_i}{\partial x_j}$, while J represents the transformation of the cell volume. The finite volume form (4) has the advantages that it is valid for both structured and unstructured meshes, and that it assures that a uniform flow exactly satisfies the equations, because $\sum_{\text{faces}} \mathbf{S} = 0$ for a closed control volume. Finite difference schemes do not necessarily satisfy this constraint because of the discretization errors in evaluating $\frac{\partial \xi_i}{\partial x_j}$ and the inversion of the transformation matrix. A cell-vertex finite volume scheme can be derived by taking the union of the cells surrounding a given vertex as the control volume for that vertex [55, 71, 139]. In equation (4), V is now the sum of the volumes of the surrounding cells, while the flux balance is evaluated over the outer faces of the polyhedral control volume. In the absence of upwind biasing the flux vector is evaluated by averaging over the corners of each face. This has the advantage of remaining accurate on an irregular or unstructured mesh. An alternative route to the discrete equations is provided by the finite element method. Whereas the finite difference and finite volume methods approximate the differential and integral operators, the finite element method proceeds by inserting an approximate solution into the exact equations. On multiplying by a test function ϕ and integrating by parts over space, one obtains the weak form

$$\frac{\partial}{\partial t}\iiint_{\Omega} \phi w d\Omega = \iiint_{\Omega} \mathbf{f}\cdot\boldsymbol{\nabla}\phi d\Omega - \iint_{\partial\Omega} \phi \mathbf{f}\cdot d\mathbf{S} \tag{6}$$

which is also valid in the presence of discontinuities in the flow. In the Galerkin method the approximate solution is expanded in terms of the same family of functions as those from which the test functions are drawn. By choosing test functions with local support, separate equations are obtained for each node. For example, if a tetrahedral mesh is used, and ϕ is piecewise linear, with a nonzero value only at a single node, the equations at each node have a stencil which contains only the nearest neighbors. In this case the finite element approximation corresponds closely to a finite volume scheme. If a piecewise linear approximation to the flux $\mathbf{f}$ is used in the evaluation of the integrals on the right hand side of equation (6), these integrals reduce to formulas which are identical to the flux balance of the finite volume scheme.

Thus the finite difference and finite volume methods lead to essentially similar schemes on structured meshes, while the finite volume method is essentially equivalent to a finite element method with linear elements when a tetrahedral mesh is used. Provided that the flow equations are expressed in the conservation law form (1), all three methods lead to an exact cancellation of the fluxes through interior cell boundaries, so that the conservative property of the equations is preserved. The important role of this

property in ensuring correct shock jump conditions was pointed out by Lax and Wendroff [97].

4.4 Non-oscillatory Shock Capturing Schemes

4.4.1 Local Extremum Diminishing (LED) Schemes

The discretization procedures which have been described in the last section lead to nondissipative approximations to the Euler equations. Dissipative terms may be needed for two reasons. The first is the possibility of undamped oscillatory modes. The second reason is the need for the clean capture of shock waves and contact discontinuities without undesirable oscillations. An extreme overshoot could result in a negative value of an inherently positive quantity such as the pressure or density. The next sections summarize a unified approach to the construction of nonoscillatory schemes via the introduction of controlled diffusive and antidiffusive terms. This is the line adhered to in the author's own work.

The development of non-oscillatory schemes has been a prime focus of algorithm research for compressible flow. Consider a general semi-discrete scheme of the form

$$\frac{d}{dt}v_j = \sum_{k\neq j} c_{jk}(v_k - v_j). \tag{7}$$

A maximum cannot increase and a minimum cannot decrease if the coefficients c_{jk} are non-negative, since at a maximum $v_k - v_j \leq 0$, and at a minimum $v_k - v_j \geq 0$. Thus the condition

$$c_{jk} \geq 0, \quad k \neq j \tag{8}$$

is sufficient to ensure stability in the maximum norm. Moreover, if the scheme has a compact stencil, so that $c_{jk} = 0$ when j and k are not nearest neighbors, a local maximum cannot increase and local minimum cannot decrease. This local extremum diminishing (LED) property prevents the birth and growth of oscillations. The one-dimensional conservation law

$$\frac{\partial u}{\partial t} + \frac{\partial}{\partial x} f(u) = 0$$

provides a useful model for analysis. In this case waves are propagated with a speed $a(u) = \frac{\partial f}{\partial u}$, and the solution is constant along the characteristics $\frac{dx}{dt} = a(u)$. Thus the LED property is satisfied. In fact the total variation

$$TV(u) = \int_{-\infty}^{\infty} \left| \frac{\partial u}{\partial x} \right| dx$$

of a solution of this equation does not increase, provided that any discontinuity appearing in the solution satisfies an entropy condition [96]. Harten proposed that difference schemes ought to be designed so that the discrete total variation cannot increase [56]. If the end values are fixed, the total variation can be expressed as

$$TV(u) = 2\left(\sum \text{ maxima } - \sum \text{ minima }\right).$$

Thus a LED scheme is also total variation diminishing (TVD). Positivity conditions of the type expressed in equations (7) and (8) lead to diagonally dominant schemes, and are the key to the elimination of improper oscillations. The positivity conditions may be realized by the introduction of diffusive terms or by the use of upwind biasing in the discrete scheme. Unfortunately, they may also lead to severe restrictions on accuracy unless the coefficients have a complex nonlinear dependence on the solution.

4.4.2 Artificial Diffusion and Upwinding

Following the pioneering work of Godunov [51], a variety of dissipative and upwind schemes designed to have good shock capturing properties have been developed during the past two decades [162, 23, 98, 100, 146, 130, 56, 129, 165, 5, 68, 182, 62, 179, 13, 12, 11]. If the one-dimensional scalar conservation law

$$\frac{\partial v}{\partial t} + \frac{\partial}{\partial x} f(v) = 0 \tag{9}$$

is represented by a three point scheme

$$\frac{dv_j}{dt} = c^+_{j+\frac{1}{2}}\left(v_{j+1} - v_j\right) + c^-_{j-\frac{1}{2}}\left(v_{j-1} - v_j\right),$$

the scheme is LED if

$$c^+_{j+\frac{1}{2}} \geq 0, \quad c^-_{j-\frac{1}{2}} \geq 0. \tag{10}$$

A conservative semidiscrete approximation to the one-dimensional conservation law can be derived by subdividing the line into cells. Then the evolution of the value v_j in the jth cell is given by

$$\Delta x \frac{dv_j}{dt} + h_{j+\frac{1}{2}} - h_{j-\frac{1}{2}} = 0, \tag{11}$$

where $h_{j+\frac{1}{2}}$ is an estimate of the flux between cells j and $j+1$. The simplest estimate is the arithmetic average $(f_{j+1} + f_j)/2$, but this leads to a scheme that does not satisfy the positivity conditions. To correct this, one may add a dissipative term and set

$$h_{j+\frac{1}{2}} = \frac{1}{2}\left(f_{j+1} + f_j\right) - \alpha_{j+\frac{1}{2}}\left(v_{j+1} - v_j\right). \tag{12}$$

In order to estimate the required value of the coefficient $\alpha_{j+\frac{1}{2}}$, let $a_{j+\frac{1}{2}}$ be a numerical estimate of the

wave speed $\frac{\partial f}{\partial u}$,

$$a_{j+\frac{1}{2}} = \begin{cases} \frac{f_{j+1}-f_j}{v_{j+1}-v_j} & \text{if} \quad v_{j+1} \neq v_j \\ \left.\frac{\partial f}{\partial v}\right|_{v=v_j} & \text{if} \quad v_{j+1} = v_j \end{cases} . \tag{13}$$

Then

$$\begin{aligned} h_{j+\frac{1}{2}} - h_{j-\frac{1}{2}} &= +\left(\frac{1}{2}a_{j+\frac{1}{2}} - \alpha_{j+\frac{1}{2}}\right)\Delta v_{j+\frac{1}{2}} \\ &\quad + \left(\frac{1}{2}a_{j-\frac{1}{2}} + \alpha_{j-\frac{1}{2}}\right)\Delta v_{j-\frac{1}{2}}, \end{aligned}$$

where

$$\Delta v_{j+\frac{1}{2}} = v_{j+1} - v_j,$$

and the LED condition (10) is satisfied if

$$\alpha_{j+\frac{1}{2}} \geq \frac{1}{2}\left|a_{j+\frac{1}{2}}\right|. \tag{14}$$

If one takes

$$\alpha_{j+\frac{1}{2}} = \frac{1}{2}\left|a_{j+\frac{1}{2}}\right|,$$

one obtains the first order upwind scheme

$$h_{j+\frac{1}{2}} = \begin{cases} f_j & \text{if } a_{j+\frac{1}{2}} > 0 \\ f_{j+1} & \text{if } a_{j+\frac{1}{2}} < 0 \end{cases} .$$

This is the least diffusive first order scheme which satisfies the LED condition. In this sense upwinding is a natural approach to the construction of non-oscillatory schemes. It may be noted that the successful treatment of transonic potential flow also involved the use of upwind biasing. This was first introduced by Murman and Cole to treat the transonic small disturbance equation [123].

Another important requirement of discrete schemes is that they should exclude nonphysical solutions which do not satisfy appropriate entropy conditions [95], which require the convergence of characteristics towards admissible discontinuities. This places more stringent bounds on the minimum level of numerical viscosity [113, 168, 128, 131]. In the case that the numerical flux function is strictly convex, Aiso has recently proved [2] that it is sufficient that

$$\alpha_{j+\frac{1}{2}} > \max\left\{\frac{1}{2}\left|a_{j+\frac{1}{2}}\right|, \epsilon \ \text{sign}(v_{j+1} - v_j)\right\}$$

for $\epsilon > 0$. Thus the numerical viscosity should be rounded out and not allowed to reach zero at a point where the wave speed $a(u) = \frac{\partial f}{\partial u}$ approaches zero. This justifies, for example, Harten's entropy fix [56].

Higher order schemes can be constructed by introducing higher order diffusive terms. Unfortunately these have larger stencils and coefficients of varying sign which are not compatible with the conditions (8) for a LED scheme, and it is known that schemes which satisfy these conditions are at best first order accurate in the neighborhood of an extremum. It proves useful in the following development to introduce the concept of essentially local extremum diminishing (ELED) schemes. These are defined to be schemes which satisfy the condition that in the limit as the mesh width $\Delta x \to 0$, local maxima are non-increasing, and local minima are non-decreasing.

4.4.3 High Resolution Switched Schemes: Jameson-Schmidt-Turkel (JST) Scheme

Higher order non-oscillatory schemes can be derived by introducing anti-diffusive terms in a controlled manner. An early attempt to produce a high resolution scheme by this approach is the Jameson-Schmidt-Turkel (JST) scheme [85]. Suppose that anti-diffusive terms are introduced by subtracting neighboring differences to produce a third order diffusive flux

$$d_{j+\frac{1}{2}} = \alpha_{j+\frac{1}{2}}\left\{\Delta v_{j+\frac{1}{2}} - \frac{1}{2}\left(\Delta v_{j+\frac{3}{2}} + \Delta v_{j-\frac{1}{2}}\right)\right\}, \tag{15}$$

which is an approximation to $\frac{1}{2}\alpha\Delta x^3\frac{\partial^3}{\partial x^3}$. The positivity condition (8) is violated by this scheme. It proves that it generates substantial oscillations in the vicinity of shock waves, which can be eliminated by switching locally to the first order scheme. The JST scheme therefore introduces blended diffusion of the form

$$\begin{aligned} d_{j+\frac{1}{2}} &= +\epsilon^{(2)}_{j+\frac{1}{2}}\Delta v_{j+\frac{1}{2}} \\ &\quad - \epsilon^{(4)}_{j+\frac{1}{2}}\left(\Delta v_{j+\frac{3}{2}} - 2\Delta v_{j+\frac{1}{2}} + \Delta v_{j-\frac{1}{2}}\right), \end{aligned} \tag{16}$$

The idea is to use variable coefficients $\epsilon^{(2)}_{j+\frac{1}{2}}$ and $\epsilon^{(4)}_{j+\frac{1}{2}}$ which produce a low level of diffusion in regions where the solution is smooth, but prevent oscillations near discontinuities. If $\epsilon^{(2)}_{j+\frac{1}{2}}$ is constructed so that it is of order Δx^2 where the solution is smooth, while $\epsilon^{(4)}_{j+\frac{1}{2}}$ is of order unity, both terms in $d_{j+\frac{1}{2}}$ will be of order Δx^3.

The JST scheme has proved very effective in practice in numerous calculations of complex steady flows, and conditions under which it could be a total variation diminishing (TVD) scheme have been examined by Swanson and Turkel [164]. An alternative statement of sufficient conditions on the coefficients $\epsilon^{(2)}_{j+\frac{1}{2}}$ and $\epsilon^{(4)}_{j+\frac{1}{2}}$ for the JST scheme to be LED is as follows:

Theorem 1 (Positivity of the JST scheme) *Suppose that whenever either v_{j+1} or v_j is an extremum the coefficients of the JST scheme satisfy*

$$\epsilon^{(2)}_{j+\frac{1}{2}} \geq \frac{1}{2}\left|\alpha_{j+\frac{1}{2}}\right|, \ \epsilon^{(4)}_{j+\frac{1}{2}} = 0. \tag{17}$$

Then the JST scheme is local extremum diminishing (LED).

Proof: *We need only consider the rate of change of v at extremal points. Suppose that v_j is an extremum. Then*

$$\epsilon^{(4)}_{j+\frac{1}{2}} = \epsilon^{(4)}_{j-\frac{1}{2}} = 0,$$

and the semi-discrete scheme (11) reduces to

$$\begin{aligned}\Delta x \frac{dv_j}{dt} &= \left(\epsilon^{(2)}_{j+\frac{1}{2}} - \frac{1}{2}a_{j+\frac{1}{2}}\right)\Delta v_{j+\frac{1}{2}} \\ &- \left(\epsilon^{(2)}_{j-\frac{1}{2}} + \frac{1}{2}a_{j-\frac{1}{2}}\right)\Delta v_{j-\frac{1}{2}},\end{aligned}$$

and each coefficient has the required sign. □

In order to construct $\epsilon^{(2)}_{j-\frac{1}{2}}$ and $\epsilon^{(4)}_{j-\frac{1}{2}}$ with the desired properties define

$$R(u,v) = \begin{cases} \left|\frac{u-v}{|u|+|v|}\right|^q & \text{if } u \neq 0 \text{ or } v \neq 0 \\ 0 & \text{if } u = v = 0, \end{cases} \quad (18)$$

where q is a positive integer. Then $R(u,v) = 1$ if u and v have opposite signs. Otherwise $R(u,v) < 1$. Now set

$$Q_j = R(\Delta v_{j+\frac{1}{2}}, \Delta v_{j-\frac{1}{2}}), \;\; Q_{j+\frac{1}{2}} = \max(Q_j, Q_{j+1}).$$

and

$$\epsilon^{(2)}_{j+\frac{1}{2}} = \alpha_{j+\frac{1}{2}} Q_{j+\frac{1}{2}}, \;\; \epsilon^{(4)}_{j+\frac{1}{2}} = \frac{1}{2}\alpha_{j+\frac{1}{2}}(1 - Q_{j+\frac{1}{2}}). \quad (19)$$

4.4.4 Symmetric Limited Positive (SLIP) Scheme

An alternative route to high resolution without oscillation is to introduce flux limiters to guarantee the satisfaction of the positivity condition (8). The use of limiters dates back to the work of Boris and Book [23]. A particularly simple way to introduce limiters, proposed by the author in 1984 [68], is to use flux limited dissipation. In this scheme the third order diffusion defined by equation (15) is modified by the insertion of limiters which produce an equivalent three point scheme with positive coefficients. The original scheme [68] can be improved in the following manner so that less restrictive flux limiters are required. Let $L(u,v)$ be a limited average of u and v with the following properties:

P1. $L(u,v) = L(v,u)$

P2. $L(\alpha u, \alpha v) = \alpha L(u,v)$

P3. $L(u,u) = u$

P4. $L(u,v) = 0$ if u and v have opposite signs: otherwise $L(u,v)$ has the same sign as u and v.

Properties (P1–P3) are natural properties of an average. Property (P4) is needed for the construction of a LED or TVD scheme.

It is convenient to introduce the notation

$$\phi(r) = L(1,r) = L(r,1),$$

where according to (P4) $\phi(r) \geq 0$. It follows from (P2) on setting $\alpha = \frac{1}{u}$ or $\frac{1}{v}$ that

$$L(u,v) = \phi\left(\frac{v}{u}\right)u = \phi\left(\frac{u}{v}\right)v.$$

Also it follows on setting $v = 1$ and $u = r$ that

$$\phi(r) = r\phi\left(\frac{1}{r}\right).$$

Thus, if there exists $r < 0$ for which $\phi(r) > 0$, then $\phi\left(\frac{1}{r}\right) < 0$. The only way to ensure that $\phi(r) \geq 0$ is to require $\phi(r) = 0$ for all $r < 0$, corresponding to property (P4).

Now one defines the diffusive flux for a scalar conservation law as

$$d_{j+\frac{1}{2}} = \alpha_{j+\frac{1}{2}}\left\{\Delta v_{j+\frac{1}{2}} - L\left(\Delta v_{j+\frac{3}{2}}, \Delta v_{j-\frac{1}{2}}\right)\right\}. \quad (20)$$

Set

$$r^+ = \frac{\Delta v_{j+\frac{3}{2}}}{\Delta v_{j-\frac{1}{2}}}, \;\; r^- = \frac{\Delta v_{j-\frac{3}{2}}}{\Delta v_{j+\frac{1}{2}}}.$$

and

$$\begin{aligned} L(\Delta v_{j+\frac{3}{2}}, \Delta v_{j-\frac{1}{2}}) &= \phi(r^+)\Delta v_{j-\frac{1}{2}} \\ L(\Delta v_{j-\frac{3}{2}}, \Delta v_{j+\frac{1}{2}}) &= \phi(r^-)\Delta v_{j+\frac{1}{2}}. \end{aligned}$$

Then,

$$\begin{aligned}\Delta x \tfrac{dv_j}{dt} &= \left\{\alpha_{j+\frac{1}{2}} - \frac{1}{2}a_{j+\frac{1}{2}} + \alpha_{j-\frac{1}{2}}\phi(r^-)\right\}\Delta v_{j+\frac{1}{2}} \\ &- \left\{\alpha_{j-\frac{1}{2}} + \frac{1}{2}a_{j-\frac{1}{2}} + \alpha_{j+\frac{1}{2}}\phi(r^+)\right\}\Delta v_{j-\frac{1}{2}} \quad (21)\end{aligned}$$

Thus the scheme satisfies the LED condition if $\alpha_{j+\frac{1}{2}} \geq \frac{1}{2}\left|a_{j+\frac{1}{2}}\right|$ for all j, and $\phi(r) \geq 0$, which is assured by property (P4) on L. At the same time it follows from property (P3) that the first order diffusive flux is canceled when Δv is smoothly varying and of constant sign. Schemes constructed by this formulation will be referred to as symmetric limited positive (SLIP) schemes. This result may be summarized as

Theorem 2 (Positivity of the SLIP scheme) *Suppose that the discrete conservation law (11) contains a limited diffusive flux as defined by equation (20). Then the positivity condition (14), together*

with the properties (P1–P4) for limited averages, are sufficient to ensure satisfaction of the LED principle that a local maximum cannot increase and a local minimum cannot decrease. □

A variety of limiters may be defined which meet the requirements of properties (P1–P4). Define

$$S(u,v) = \frac{1}{2}\left\{\text{sign}(u) + \text{sign}(v)\right\}$$

which vanishes is u and v have opposite signs.

Then two limiters which are appropriate are the following well-known schemes:

1. Minmod:

$$L(u,v) = S(u,v)\min(|u|,|v|)$$

2. Van Leer:

$$L(u,v) = S(u,v)\frac{2|u||v|}{|u|+|v|}.$$

In order to produce a family of limiters which contains these as special cases it is convenient to set

$$L(u,v) = \frac{1}{2}D(u,v)(u+v),$$

where $D(u,v)$ is a factor which should deflate the arithmetic average, and become zero if u and v have opposite signs. Take

$$D(u,v) = 1 - R(u,v) = 1 - \left|\frac{u-v}{|u|+|v|}\right|^q, \qquad (22)$$

where $R(u,v)$ is the same function that was introduced in the JST scheme, and q is a positive integer. Then $D(u,v) = 0$ if u and v have opposite signs. Also if $q = 1$, $L(u,v)$ reduces to minmod, while if $q = 2$, $L(u,v)$ is equivalent to Van Leer's limiter. By increasing q one can generate a sequence of limited averages which approach a limit defined by the arithmetic mean truncated to zero when u and v have opposite signs.

When the terms are regrouped, it can be seen that with this limiter the SLIP scheme is exactly equivalent to the JST scheme, with the switch is defined as

$$\begin{aligned} Q_{j+\frac{1}{2}} &= R\left(\Delta v_{j+\frac{3}{2}}, \Delta v_{j+\frac{1}{2}}\right) \\ \epsilon^{(2)}_{j+\frac{1}{2}} &= \alpha_{j+\frac{1}{2}} Q_{j+\frac{1}{2}} \\ \epsilon^{(4)}_{j+\frac{1}{2}} &= \alpha_{j+\frac{1}{2}}\left(1 - Q_{j+\frac{1}{2}}\right). \end{aligned}$$

This formulation thus unifies the JST and SLIP schemes.

4.4.5 Essentially Local Extremum Diminishing (ELED) Scheme with Soft Limiter

The limiters defined by the formula (22) have the disadvantage that they are active at a smooth extrema, reducing the local accuracy of the scheme to first order. In order to prevent this, the SLIP scheme can be relaxed to give an essentially local extremum diminishing (ELED) scheme which is second order accurate at smooth extrema by the introduction of a threshold in the limited average. Therefore redefine $D(u,v)$ as

$$D(u,v) = 1 - \left|\frac{u-v}{\max(|u|+|v|, \epsilon\Delta x^r)}\right|^q, \qquad (23)$$

where $r = \frac{3}{2}$, $q \geq 2$. This reduces to the previous definition if $|u|+|v| > \epsilon\Delta x^r$.

In any region where the solution is smooth, $\Delta v_{j+\frac{3}{2}} - \Delta v_{j-\frac{1}{2}}$ is of order Δx^2. In fact if there is a smooth extremum in the neighborhood of v_j or v_{j+1}, a Taylor series expansion indicates that $\Delta v_{j+\frac{3}{2}}$, $\Delta v_{j+\frac{1}{2}}$ and $\Delta v_{j-\frac{1}{2}}$ are each individually of order Δx^2, since $\frac{dv}{dx} = 0$ at the extremum. It may be verified that second order accuracy is preserved at a smooth extremum if $q \geq 2$. On the other hand the limiter acts in the usual way if $\left|\Delta v_{j+\frac{3}{2}}\right|$ or $\left|\Delta v_{j-\frac{3}{2}}\right| > \epsilon\Delta x^r$, and it may also be verified that in the limit $\Delta x \to 0$ local maxima are non increasing and local minima are non decreasing [79]. Thus the scheme is essentially local extremum diminishing (ELED).

The effect of the "soft limiter" is not only to improve the accuracy: the introduction of a threshold below which extrema of small amplitude are accepted also usually results in a faster rate of convergence to a steady state, and decreases the likelyhood of limit cycles in which the limiter interacts unfavorably with the corrections produced by the updating scheme. In a scheme recently proposed by Venkatakrishnan a threshold is introduced precisely for this purpose [173].

4.4.6 Upstream Limited Positive (USLIP) Schemes

By adding the anti-diffusive correction purely from the upstream side one may derive a family of upstream limited positive (USLIP) schemes. Corresponding to the original SLIP scheme defined by equation (20), a USLIP scheme is obtained by setting

$$d_{j+\frac{1}{2}} = \alpha_{j+\frac{1}{2}}\left\{\Delta v_{j+\frac{1}{2}} - L\left(\Delta v_{j+\frac{1}{2}}, \Delta v_{j-\frac{1}{2}}\right)\right\}$$

if $a_{j+\frac{1}{2}} > 0$, or

$$d_{j+\frac{1}{2}} = \alpha_{j+\frac{1}{2}}\left\{\Delta v_{j+\frac{1}{2}} - L\left(\Delta v_{j+\frac{1}{2}}, \Delta v_{j+\frac{3}{2}}\right)\right\}$$

if $a_{j+\frac{1}{2}} < 0$. If $\alpha_{j+\frac{1}{2}} = \frac{1}{2}\left|a_{j+\frac{1}{2}}\right|$ one recovers a standard high resolution upwind scheme in semi-discrete form. Consider the case that $a_{j+\frac{1}{2}} > 0$ and $a_{j-\frac{1}{2}} > 0$. If one sets

$$r^+ = \frac{\Delta v_{j+\frac{1}{2}}}{\Delta v_{j-\frac{1}{2}}}, \quad r^- = \frac{\Delta v_{j-\frac{3}{2}}}{\Delta v_{j-\frac{1}{2}}},$$

the scheme reduces to

$$\Delta x \frac{dv_j}{dt} = -\frac{1}{2}\left\{\phi(r^+)a_{j+\frac{1}{2}} + \left(2 - \phi(r^-)\right)a_{j-\frac{1}{2}}\right\}\Delta v_{j-\frac{1}{2}}.$$

To assure the correct sign to satisfy the LED criterion the flux limiter must now satisfy the additional constraint that $\phi(r) \leq 2$.

The USLIP formulation is essentially equivalent to standard upwind schemes [130, 165]. Both the SLIP and USLIP constructions can be implemented on unstructured meshes [75, 79]. The anti-diffusive terms are then calculated by taking the scalar product of the vectors defining an edge with the gradient in the adjacent upstream and downstream cells.

4.4.7 Systems of Conservation Laws: Flux Splitting and Flux-Difference Splitting

Steger and Warming [162] first showed how to generalize the concept of upwinding to the system of conservation laws

$$\frac{\partial w}{\partial t} + \frac{\partial}{\partial x} f(w) = 0 \tag{24}$$

by the concept of flux splitting. Suppose that the flux is split as $f = f^+ + f^-$ where $\frac{\partial f^+}{\partial w}$ and $\frac{\partial f^-}{\partial w}$ have positive and negative eigenvalues. Then the first order upwind scheme is produced by taking the numerical flux to be

$$h_{j+\frac{1}{2}} = f_j^+ + f_{j+1}^-.$$

This can be expressed in viscosity form as

$$\begin{aligned} h_{j+\frac{1}{2}} &= \frac{1}{2}\left(f_{j+1}^+ + f_j^+\right) - \frac{1}{2}\left(f_{j+1}^+ - f_j^+\right) \\ &\quad + \frac{1}{2}\left(f_{j+1}^- + f_j^-\right) + \frac{1}{2}\left(f_{j+1}^- - f_j^-\right) \\ &= \frac{1}{2}\left(f_{j+1} + f_j\right) - d_{j+\frac{1}{2}}, \end{aligned}$$

where the diffusive flux is

$$d_{j+\frac{1}{2}} = \frac{1}{2}\Delta(f^+ - f^-)_{j+\frac{1}{2}}. \tag{25}$$

Roe derived the alternative formulation of flux difference splitting [146] by distributing the corrections due to the flux difference in each interval upwind and downwind to obtain

$$\Delta x \frac{dw_j}{dt} + (f_{j+1} - f_j)^- + (f_j - f_{j-1})^+ = 0,$$

where now the flux difference $f_{j+1} - f_j$ is split. The corresponding diffusive flux is

$$d_{j+\frac{1}{2}} = \frac{1}{2}\left(\Delta f_{j+\frac{1}{2}}^+ - \Delta f_{j+\frac{1}{2}}^-\right).$$

Following Roe's derivation, let $A_{j+\frac{1}{2}}$ be a mean value Jacobian matrix exactly satisfying the condition

$$f_{j+1} - f_j = A_{j+\frac{1}{2}}(w_{j+1} - w_j). \tag{26}$$

$A_{j+\frac{1}{2}}$ may be calculated by substituting the weighted averages

$$u = \frac{\sqrt{\rho_{j+1}}u_{j+1} + \sqrt{\rho_j}u_j}{\sqrt{\rho_{j+1}} + \sqrt{\rho_j}}, H = \frac{\sqrt{\rho_{j+1}}H_{j+1} + \sqrt{\rho_j}H_j}{\sqrt{\rho_{j+1}} + \sqrt{\rho_j}} \tag{27}$$

into the standard formulas for the Jacobian matrix $A = \frac{\partial f}{\partial w}$. A splitting according to characteristic fields is now obtained by decomposing $A_{j+\frac{1}{2}}$ as

$$A_{j+\frac{1}{2}} = T\Lambda T^{-1}, \tag{28}$$

where the columns of T are the eigenvectors of $A_{j+\frac{1}{2}}$, and Λ is a diagonal matrix of the eigenvalues. Now the corresponding diffusive flux is

$$\frac{1}{2}\left|A_{j+\frac{1}{2}}\right|(w_{j+1} - w_j),$$

where

$$\left|A_{j+\frac{1}{2}}\right| = T\left|\Lambda\right|T^{-1}$$

and $|\Lambda|$ is the diagonal matrix containing the absolute values of the eigenvalues.

4.4.8 Alternative Splittings

Characteristic splitting has the advantages that it introduces the minimum amount of diffusion to exclude the growth of local extrema of the characteristic variables, and that with the Roe linearization it allows a discrete shock structure with s single interior point. To reduce the computational complexity one may replace $|A|$ by αI where if α is at least equal to the spectral radius $\max|\lambda(A)|$, then the positivity conditions will still be satisfied. Then the first order scheme simply has the scalar diffusive flux

$$d_{j+\frac{1}{2}} = \frac{1}{2}\alpha_{j+\frac{1}{2}}\Delta w_{j+\frac{1}{2}}. \tag{29}$$

The JST scheme with scalar diffusive flux captures shock waves with about 3 interior points, and it has been widely used for transonic flow calculations because it is both robust and computationally inexpensive.

An intermediate class of schemes can be formulated by defining the first order diffusive flux as a combination of differences of the state and flux vectors

$$d_{j+\frac{1}{2}} = \frac{1}{2}\alpha_{j+\frac{1}{2}}^* c\left(w_{j+1} - w_j\right) + \frac{1}{2}\beta_{j+\frac{1}{2}}\left(f_{j+1} - f_j\right), \tag{30}$$

where the factor c is included in the first term to make $\alpha^*_{j+\frac{1}{2}}$ and $\beta_{j+\frac{1}{2}}$ dimensionless. Schemes of this class are fully upwind in supersonic flow if one takes $\alpha^*_{j+\frac{1}{2}} = 0$ and $\beta_{j+\frac{1}{2}} = \text{sign}(M)$ when the absolute value of the Mach number M exceeds 1. The flux vector f can be decomposed as

$$f = uw + f_p, \tag{31}$$

where

$$f_p = \begin{pmatrix} 0 \\ p \\ up \end{pmatrix}. \tag{32}$$

Then

$$f_{j+1} - f_j = \bar{u}\,(w_{j+1} - w_j) + \bar{w}\,(u_{j+1} - u_j) + f_{p_{j+1}} - f_{p_j}, \tag{33}$$

where $\bar{u}$ and $\bar{w}$ are the arithmetic averages

$$\bar{u} = \frac{1}{2}\,(u_{j+1} + u_j)\,, \quad \bar{w} = \frac{1}{2}\,(w_{j+1} + w_j)\,.$$

Thus these schemes are closely related to schemes which introduce separate splittings of the convective and pressure terms, such as the wave-particle scheme [141, 8], the advection upwind splitting method (AUSM) [106, 175], and the convective upwind and split pressure (CUSP) schemes [76].

In order to examine the shock capturing properties of these various schemes, consider the general case of a first order diffusive flux of the form

$$d_{j+\frac{1}{2}} = \frac{1}{2}\alpha_{j+\frac{1}{2}} B_{j+\frac{1}{2}}\,(w_{j+1} - w_j)\,, \tag{34}$$

where the matrix $B_{j+\frac{1}{2}}$ determines the properties of the scheme and the scaling factor $\alpha_{j+\frac{1}{2}}$ is included for convenience. All the previous schemes can be obtained by representing $B_{j+\frac{1}{2}}$ as a polynomial in the matrix $A_{j+\frac{1}{2}}$ defined by equation (26). Schemes of this class were considered by Van Leer [99]. According to the Cayley-Hamilton theorem, a matrix satisfies its own characteristic equation. Therefore the third and higher powers of A can be eliminated, and there is no loss of generality in limiting $B_{j+\frac{1}{2}}$ to a polynomial of degree 2,

$$B_{j+\frac{1}{2}} = \alpha_0 I + \alpha_1 A_{j+\frac{1}{2}} + \alpha_2 A^2_{j+\frac{1}{2}}. \tag{35}$$

The characteristic upwind scheme for which $B_{j+\frac{1}{2}} = \left|A_{j+\frac{1}{2}}\right|$ is obtained by substituting $A_{j+\frac{1}{2}} = T\Lambda T^{-1}$, $A^2_{j+\frac{1}{2}} = T\Lambda^2 T^{-1}$. Then α_0, α_1, and α_2 are determined from the three equations

$$\alpha_0 + \alpha_1\lambda_k + \alpha_2\lambda_k^2 = |\lambda_k|\,, \quad k = 1, 2, 3.$$

The same representation remains valid for three dimensional flow because $A_{j+\frac{1}{2}}$ still has only three distinct eigenvalues u, $u + c$, $u - c$.

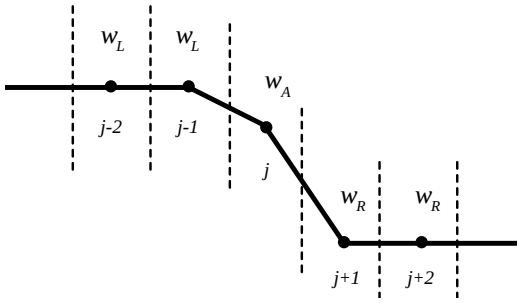

Figure 4: Shock structure for single interior point.

4.4.9 Analysis of Stationary Discrete Shocks

The ideal model of a discrete shock is illustrated in figure (4). Suppose that w_L and w_R are left and right states which satisfy the jump conditions for a stationary shock, and that the corresponding fluxes are $f_L = f(w_L)$ and $f_R = f(w_R)$. Since the shock is stationary $f_L = f_R$. The ideal discrete shock has constant states w_L to the left and w_R to the right, and a single point with an intermediate value w_A. The intermediate value is needed to allow the discrete solution to correspond to a true solution in which the shock wave does not coincide with an interface between two mesh cells.

Schemes corresponding to one, two or three terms in equation (35) are examined in [80]. The analysis of these three cases shows that a discrete shock structure with a single interior point is supported by artificial diffusion that satisfies the two conditions that

1. it produces an upwind flux if the flow is determined to be supersonic through the interface
2. it satisfies a generalized eigenvalue problem for the exit from the shock of the form

$$(A_{AR} - \alpha_{AR} B_{AR})\,(w_R - w_A) = 0, \tag{36}$$

where A_{AR} is the linearized Jacobian matrix and B_{AR} is the matrix defining the diffusion for the interface AR. This follows from the equilibrium condition $h_{RA} = h_{RR}$ for the cell $j+1$ in figure 4. These two conditions are satisfied by both the characteristic scheme and also the CUSP scheme, provided that the coefficients of convective diffusion and pressure differences are correctly balanced. Scalar diffusion does not satisfy the first condition. In the case of the CUSP scheme (30) equation 36 reduces to

$$\left(A_{RA} + \frac{\alpha^* c}{1+\beta}\right)(w_R - w_A) = 0$$

Thus $w_R - w_A$ is an eigenvector of the Roe matrix A_{RA}, and $-\frac{\alpha^* c}{1+\beta}$ is the corresponding eigenvalue. Since the eigenvalues are u, $u+c$, and $u-c$, the only choice which leads to positive diffusion when $u > 0$ is $u - c$, yielding the relationship

$$\alpha^* c = (1+\beta)(c-u), 0 < u < c$$

Thus there is a one parameter family of schemes which support the ideal shock structure. The term $\beta(f_R - f_A)$ contributes to the diffusion of the convective terms. Allowing for the split (31), the total effective coefficient of convective diffusion is $\alpha c = \alpha^* c + \beta\overline{u}$. A CUSP scheme with low numerical diffusion is then obtained by taking $\alpha = |M|$, leading to the coefficients illustrated in figure 5

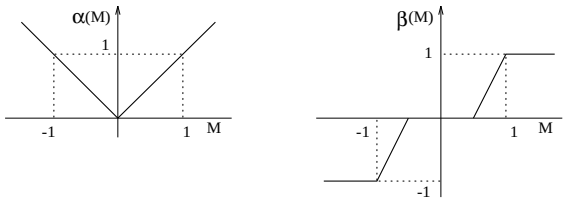

Figure 5: Diffusion Coefficients.

4.4.10 CUSP and Characteristic Schemes Admitting Constant Total Enthalpy in Steady Flow

In steady flow the stagnation enthalpy H is constant, corresponding to the fact that the energy and mass conservation equations are consistent when the constant factor H is removed from the energy equation. Discrete and semi-discrete schemes do not necessarily satisfy this property. In the case of a semi-discrete scheme expressed in viscosity form, equations (11) and (12), a solution with constant H is admitted if the viscosity for the energy equation reduces to the viscosity for the continuity equation with ρ replaced by ρH. When the standard characteristic decomposition (28) is used, the viscous fluxes for ρ and ρH which result from composition of the fluxes for the characteristic variables do not have this property, and H is not constant in the discrete solution. In practice there is an excursion of H in the discrete shock structure which represents a local heat source. In very high speed flows the corresponding error in the temperature may lead to a wrong prediction of associated effects such as chemical reactions.

The source of the error in the stagnation enthalpy is the discrepancy between the convective terms

$$u \begin{pmatrix} \rho \\ \rho u \\ \rho H \end{pmatrix},$$

in the flux vector, which contain ρH, and the state vector which contains ρE. This may be remedied by introducing a modified state vector

$$w_h = \begin{pmatrix} \rho \\ \rho u \\ \rho H \end{pmatrix}.$$

Then one introduces the linearization

$$f_R - f_L = A_h(w_{h_R} - w_{h_L}).$$

Here A_h may be calculated in the same way as the standard Roe linearization. Introduce the weighted averages defined by equation (27). Then

$$A_h = \begin{pmatrix} 0 & 1 & 0 \\ -\frac{\gamma+1}{\gamma}\frac{u^2}{2} & \frac{\gamma+1}{\gamma}u & \frac{\gamma-1}{\gamma} \\ -uH & H & u \end{pmatrix}.$$

The eigenvalues of A_h are u, λ^+ and λ^- where

$$\lambda^{\pm} = \frac{\gamma+1}{2\gamma}u \pm \sqrt{(\frac{\gamma+1}{2\gamma}u)^2 + \frac{c^2-u^2}{\gamma}}. \qquad (37)$$

Now both CUSP and characteristic schemes which preserve constant stagnation enthalpy in steady flow can be constructed from the modified Jacobian matrix A_h [80]. These schemes also produce a discrete shock structure with one interior point in steady flow. Then one arrives at four variations with this property, which can conveniently be distinguished as the E- and H-CUSP schemes, and the E- and H-characteristic schemes.

4.5 Multidimensional Schemes

The simplest approach to the treatment of multidimensional problems on structured meshes is to apply the one-dimensional construction separately in each mesh direction. On triangulated meshes in two or three dimensions the SLIP and USLIP constructions may also be implemented along the mesh edges [79]. A substantial body of current research is directed toward the implementation of truly multidimensional upwind schemes in which the upwind biasing is determined by properties of the flow rather than the mesh. A thorough review is given by Pailliere and DeConinck in reference [132].

Residual distribution schemes are an attractive approach for triangulated meshes. In these the residual defined by the space derivatives is evaluated for

each cell, and then distributed to the vertices with weights which depend on the direction of convection. For a scalar conservation law the weights can be chosen to maintain positivity with minimum cross diffusion in the direction normal to the flow. For the Euler equations the residual can be linearized by assuming that the parameter vector with components $\sqrt{\rho}$,$\sqrt{\rho}u_i$, and $\sqrt{\rho}H$ varies linearly over the cell. Then

$$\frac{\partial f_j(w)}{\partial x_j} = A_j \frac{\partial w}{\partial x_j}$$

where the Jacobian matrices $A_j = \frac{\partial f_j}{\partial w}$ are evaluated with Roe averaging of the values of w at the vertices. Waves in the direction $\mathbf{n}$ can then be expressed in terms of the eigenvectors of $n_j A_j$, and a positive distribution scheme is used for waves in preferred directions. The best choice of these directions is the subject of ongoing research, but preliminary results indicate the possibility of achieving high resolution of shocks and contact discontinuities which are not aligned with mesh lines [132].

Hirsch and Van Ransbeeck adopt an alternative approach in which they directly construct directional diffusive terms on structured meshes, with anti-diffusion controlled by limiters based on comparisons of slopes in different directions [60]. They also show promising results in calculations of nozzles with multiply reflected oblique shocks.

4.5.1 High Order Godunov Schemes, and Kinetic Flux Splitting

A substantial body of current research is directed toward the implementation of truly multi-dimensional upwind schemes [59, 135, 101]. Reference [132] provides a thorough review of recent developments in this field. Some of the most impressive simulations of time dependent flows with strong shock waves have been achieved with higher order Godunov schemes [179]. In these schemes the average value in each cell is updated by applying the integral conservation law using interface fluxes predicted from the exact or approximate solution of a Riemann problem between adjacent cells. A higher order estimate of the solution is then reconstructed from the cell averages, and slope limiters are applied to the reconstruction. An example is the class of essentially non-oscillatory (ENO) schemes, which can attain a very high order of accuracy at the cost of a substantial increase in computational complexity [32, 153, 151, 152]. Methods based on reconstruction can also be implemented on unstructured meshes [13, 12]. Recently there has been an increasing interest in kinetic flux splitting schemes, which use solutions of the Boltzmann equation or the BGK equation to predict the interface fluxes [42, 36, 45, 136, 180].

4.6 Discretization of the Viscous Terms

The discretization of the viscous terms of the Navier Stokes equations requires an approximation to the velocity derivatives $\frac{\partial u_i}{\partial x_j}$ in order to calculate the tensor σ_{ij}, equation (3). Then the viscous terms may be included in the flux balance (4). In order to evaluate the derivatives one may apply the Gauss formula to a control volume V with the boundary S.

$$\int_V \frac{\partial u_i}{\partial x_j} dv = \int_S u_i n_j ds$$

where n_j is the outward normal. For a tetrahedral or hexahedral cell this gives

$$\overline{\frac{\partial u_i}{\partial x_j}} = \frac{1}{\text{vol}} \sum_{\text{faces}} \overline{u}_i \; n_j \; s \tag{38}$$

where $\overline{u}_i$ is an estimate of the average of u_i over the face. If u varies linearly over a tetrahedral cell this is exact. Alternatively, assuming a local transformation to computational coordinates ξ_j, one may apply the chain rule

$$\frac{\partial u}{\partial x} = \left[\frac{\partial u}{\partial \xi}\right] \left[\frac{\partial \xi}{\partial x}\right] = \frac{\partial u}{\partial \xi} \left[\frac{\partial x}{\partial \xi}\right]^{-1} \tag{39}$$

Here the transformation derivatives $\frac{\partial x_i}{\partial \xi_j}$ can be evaluated by the same finite difference formulas as the velocity derivatives $\frac{\partial u_i}{\partial \xi_j}$ In this case $\frac{\partial u}{\partial \xi}$ is exact if u is a linearly varying function.

For a cell-centered discretization (figure 6a) $\frac{\partial u}{\partial \xi}$ is needed at each face. The simplest procedure is to evaluate $\frac{\partial u}{\partial \xi}$ in each cell, and to average $\frac{\partial u}{\partial \xi}$ between the two cells on either side of a face [87]. The resulting discretization does not have a compact stencil, and supports undamped oscillatory modes. In a one dimensional calculation, for example, $\frac{\partial^2 u}{\partial x^2}$ would be discretized as $\frac{u_{i+2}-2u_i+u_{i-2}}{4\Delta x^2}$. In order to produce a compact stencil $\frac{\partial u}{\partial x}$ may be estimated from a control volume centered on each face, using formulas (38) or (39) [144]. This is computationally expensive because the number of faces is much larger than the number of cells. In a hexahedral mesh with a large number of vertices the number of faces approaches three times the number of cells.

This motivates the introduction of dual meshes for the evaluation of the velocity derivatives and the flux balance as sketched in figure 6. The figure shows both cell-centered and cell-vertex schemes. The dual mesh connects cell centers of the primary mesh. If there is a kink in the primary mesh, the dual cells

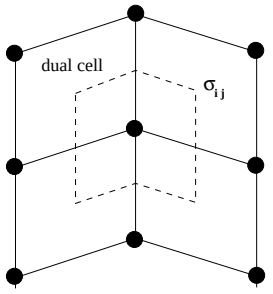

6a: Cell-centered scheme. σ_{ij} evaluated at vertices of the primary mesh

6b: Cell-vertex scheme. σ_{ij} evaluated at cell centers of the primary mesh

Figure 6: Viscous discretizations for cell-centered and cell-vertex algorithms.

should be formed by assembling contiguous fractions of the neighboring primary cells. On smooth meshes comparable results are obtained by either of these formulations [114, 115, 107]. If the mesh has a kink the cell-vertex scheme has the advantage that the derivatives $\frac{\partial u_i}{\partial x_j}$ are calculated in the interior of a regular cell, with no loss of accuracy.

A desirable property is that a linearly varying velocity distribution, as in a Couette flow, should produce a constant stress and hence an exact stress balance. This property is not necessarily satisfied in general by finite difference or finite volume schemes on curvilinear meshes. The characterization k-exact has been proposed for schemes that are exact for polynomials of degree k. The cell-vertex finite volume scheme is linearly exact if the derivatives are evaluated by equation (39), since then $\frac{\partial u_i}{\partial x_j}$ is exactly evaluated as a constant, leading to constant viscous stresses σ_{ij}, and an exact viscous stress balance. This remains true when there is a kink in the mesh, because the summation of constant stresses over the faces of the kinked control volume sketched in figure 6 still yields a perfect balance. The use of equation (39) to evaluate $\frac{\partial u_i}{\partial x_j}$, however, requires the additional calculation or storage of the nine metric quantities $\frac{\partial u_i}{\partial x_j}$ in each cell, whereas equation (38) can be evaluated from the same face areas that are used for the flux balance.

In the case of an unstructured mesh, the weak form (6) leads to a natural discretization with linear elements, in which the piecewise linear approximation yields a constant stress in each cell. This method yields a representation which is globally correct when averaged over the cells, as is proved by energy estimates for elliptic problems [15]. It should be noted, however, that it yields formulas that are not necessarily locally consistent with the differential equations, if Taylor series expansions are substituted for the solution at the vertices appearing in the local stencil. Figure 7 illustrates the discretization of the Laplacian $u_{xx} + u_{yy}$ which is obtained with linear elements. It shows a particular triangulation such that the approximation is locally consistent with $u_{xx} + 3u_{yy}$. Thus the use of an irregular triangulation in the boundary layer may significantly degrade the accuracy.

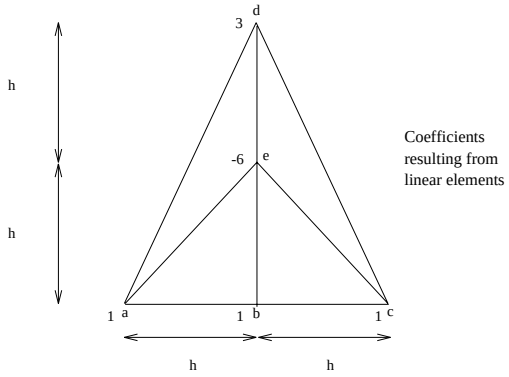

Figure 7: Example of discretization $u_{xx} + u_{yy}$ on a triangular mesh. The discretization is locally equivalent to the approximation $u_{xx} = \frac{u_a - 2u_b + u_c}{h^2}, 3u_{yy} = \frac{3u_d - 6u_e + 3u_b}{h^2}$.

4.7 Time Stepping Schemes

If the space discretization procedure is implemented separately, it leads to a set of coupled ordinary differential equations, which can be written in the form

$$\frac{d\mathbf{w}}{dt} + \mathbf{R}(\mathbf{w}) = \mathbf{0}, \tag{40}$$

where $\mathbf{w}$ is the vector of the flow variables at the mesh points, and $\mathbf{R}(\mathbf{w})$ is the vector of the residuals, consisting of the flux balances defined by the space discretization scheme, together with the added dissipative terms. If the objective is simply to reach the steady state and details of the transient solution are immaterial, the time-stepping scheme may be designed solely to maximize the rate of convergence. The first decision that must be made is whether to use an explicit scheme, in which the space derivatives are calculated from known values of the flow variables at the beginning of the time step, or an implicit scheme, in which the formulas for the space derivatives include as yet unknown values of the flow variables at the end of the time step, leading to the need to solve coupled equations for the new values. The permissible time step for an explicit scheme is limited by the Courant-Friedrichs-Lewy (CFL) condition, which states that a difference scheme cannot be a convergent and stable approximation unless its

domain of dependence contains the domain of dependence of the corresponding differential equation. One can anticipate that implicit schemes will yield convergence in a smaller number of time steps, because the time step is no longer constrained by the CFL condition. Implicit schemes will be efficient, however, only if the decrease in the number of time steps outweighs the increase in the computational effort per time step consequent upon the need to solve coupled equations. The prototype implicit scheme can be formulated by estimating $\frac{\partial \mathbf{W}}{\partial t}$ at $t + \mu\Delta t$ as a linear combination of $\mathbf{R}(\mathbf{w^n})$ and $\mathbf{R}(\mathbf{w^{n+1}})$. The resulting equation

$$\mathbf{w}^{n+1} = \mathbf{w}^n - \Delta t \left\{ (1-\mu)\, \mathbf{R}\left(\mathbf{w^n}\right) + \mu \mathbf{R}\left(\mathbf{w}^{n+1}\right) \right\}$$

can be linearized as

$$\left(\mathbf{I} + \mu \Delta t \frac{\partial \mathbf{R}}{\partial \mathbf{w}} \right) \delta \mathbf{w} + \Delta t \mathbf{R}\left(\mathbf{w}^n\right) = 0.$$

If one sets $\mu = 1$ and lets $\Delta t \to \infty$ this reduces to the Newton iteration , which has been successfully used in two-dimensional calculations [172, 50]. In the three-dimensional case with, say, an $N \times N \times N$ mesh, the bandwidth of the matrix that must be inverted is of order N^2. Direct inversion requires a number of operations proportional to the number of unknowns multiplied by the square of the bandwidth of the order of N^7. This is prohibitive, and forces recourse to either an approximate factorization method or an iterative solution method.

Alternating direction methods, which introduce factors corresponding to each coordinate, are widely used for structured meshes [17, 137]. They cannot be implemented on unstructured tetrahedral meshes that do not contain identifiable mesh directions, although other decompositions are possible [108]. If one chooses to adopt the iterative solution technique, the principal alternatives are variants of the Gauss-Seidel and Jacobi methods. A symmetric Gauss-Seidel method with one iteration per time step is essentially equivalent to an approximate lower-upper (LU) factorization of the implicit scheme [86, 125, 31, 183]. On the other hand, the Jacobi method with a fixed number of iterations per time step reduces to a multistage explicit scheme, belonging to the general class of Runge-Kutta schemes [33]. Schemes of this type have proved very effective for wide variety of problems, and they have the advantage that they can be applied equally easily on both structured and unstructured meshes [84, 67, 69, 145].

If one reduces the linear model problem corresponding to (40) to an ordinary differential equation by substituting a Fourier mode $\hat{w} = e^{ipx_j}$, the resulting Fourier symbol has an imaginary part proportional to the wave speed, and a negative real part proportional to the diffusion. Thus the time stepping scheme should have a stability region which contains a substantial interval of the negative real axis, as well as an interval along the imaginary axis. To achieve this it pays to treat the convective and dissipative terms in a distinct fashion. Thus the residual is split as

$$R(w) = Q(w) + D(w),$$

where $Q(w)$ is the convective part and $D(w)$ the dissipative part. Denote the time level $n\Delta t$ by a superscript n. Then the multistage time stepping scheme is formulated as

$$\begin{aligned} w^{(n+1,0)} &= w^n \\ &\cdots \\ w^{(n+1,k)} &= w^n - \alpha_k \Delta t \left(Q^{(k-1)} + D^{(k-1)} \right) \\ &\cdots \\ w^{n+1} &= w^{(n+1,m)}, \end{aligned}$$

where the superscript k denotes the k-th stage, $\alpha_m = 1$, and

$$\begin{aligned} Q^{(0)} &= Q\left(w^n\right), \;\; D^{(0)} = D\left(w^n\right) \\ &\cdots \\ Q^{(k)} &= Q\left(w^{(n+1,k)}\right) \\ D^{(k)} &= \beta_k D\left(w^{(n+1,k)}\right) + (1-\beta_k) D^{(k-1)}. \end{aligned}$$

The coefficients α_k are chosen to maximize the stability interval along the imaginary axis, and the coefficients β_k are chosen to increase the stability interval along the negative real axis.

These schemes do not fall within the standard framework of Runge-Kutta schemes, and they have much larger stability regions [69]. Two schemes which have been found to be particularly effective are tabulated below. The first is a four-stage scheme with two evaluations of dissipation. Its coefficients are

$$\begin{array}{ll} \alpha_1 = \frac{1}{3} & \beta_1 = 1 \\ \alpha_2 = \frac{4}{15} & \beta_2 = \frac{1}{2} \\ \alpha_3 = \frac{5}{9} & \beta_3 = 0 \\ \alpha_4 = 1 & \beta_4 = 0 \end{array} . \tag{41}$$

The second is a five-stage scheme with three evaluations of dissipation. Its coefficients are

$$\begin{array}{ll} \alpha_1 = \frac{1}{4} & \beta_1 = 1 \\ \alpha_2 = \frac{1}{6} & \beta_2 = 0 \\ \alpha_3 = \frac{3}{8} & \beta_3 = 0.56 \\ \alpha_4 = \frac{1}{2} & \beta_4 = 0 \\ \alpha_5 = 1 & \beta_5 = 0.44 \end{array} . \tag{42}$$

4.8 Multigrid Methods

4.8.1 Acceleration of Steady Flow Calculations

Radical improvements in the rate of convergence to a steady state can be realized by the multigrid time-

stepping technique. The concept of acceleration by the introduction of multiple grids was first proposed by Fedorenko [48]. There is by now a fairly well-developed theory of multigrid methods for elliptic equations based on the concept that the updating scheme acting as a smoothing operator on each grid [24, 53]. This theory does not hold for hyperbolic systems. Nevertheless, it seems that it ought to be possible to accelerate the evolution of a hyperbolic system to a steady state by using large time steps on coarse grids so that disturbances will be more rapidly expelled through the outer boundary. Various multigrid time-stepping schemes designed to take advantage of this effect have been proposed [124, 65, 55, 71, 29, 6, 57, 83, 93].

One can devise a multigrid scheme using a sequence of independently generated coarser meshes by eliminating alternate points in each coordinate direction. In order to give a precise description of the multigrid scheme, subscripts may be used to indicate the grid. Several transfer operations need to be defined. First the solution vector on grid k must be initialized as

$$w_k^{(0)} = T_{k,k-1} w_{k-1},$$

where w_{k-1} is the current value on grid $k-1$, and $T_{k,k-1}$ is a transfer operator. Next it is necessary to transfer a residual forcing function such that the solution grid k is driven by the residuals calculated on grid $k-1$. This can be accomplished by setting

$$P_k = Q_{k,k-1} R_{k-1}\left(w_{k-1}\right) - R_k\left[w_k^{(0)}\right],$$

where $Q_{k,k-1}$ is another transfer operator. Then $R_k(w_k)$ is replaced by $R_k(w_k)+P_k$ in the time- stepping scheme. Thus, the multistage scheme is reformulated as

$$\begin{aligned} w_k^{(1)} &= w_k^{(0)} - \alpha_1 \Delta t_k \left[R_k^{(0)} + P_k\right] \\ \cdots &\quad \cdots \\ w_k^{(q+1)} &= w_k^{(0)} - \alpha_{q+1} \Delta t_k \left[R_k^{(q)} + P_k\right]. \end{aligned}$$

The result $w_k^{(m)}$ then provides the initial data for grid $k+1$. Finally, the accumulated correction on grid k has to be transferred back to grid $k-1$ with the aid of an interpolation operator $I_{k-1,k}$. With properly optimized coefficients multistage time-stepping schemes can be very efficient drivers of the multigrid process. A W-cycle of the type illustrated in Figure 8 proves to be a particularly effective strategy for managing the work split between the meshes. In a three-dimensional case the number of cells is reduced by a factor of eight on each coarser grid. On examination of the figure, it can therefore be seen that the work measured in units corresponding to a step on the fine grid is of the order of

$$1 + 2/8 + 4/64 + \ldots < 4/3,$$

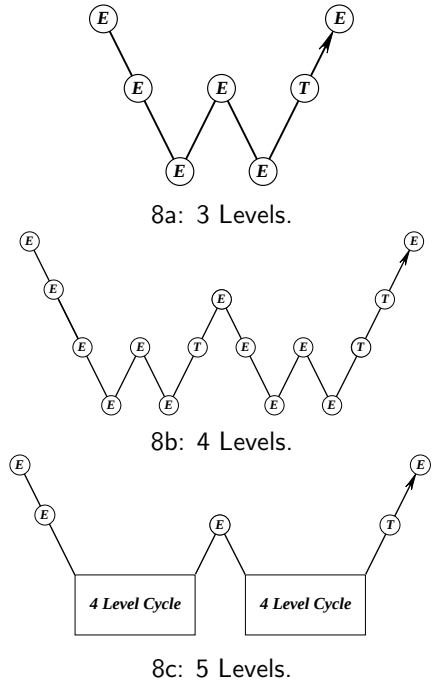

Figure 8: Multigrid W-cycle for managing the grid calculation. E, evaluate the change in the flow for one step; T, transfer the data without updating the solution.

and consequently the very large effective time step of the complete cycle costs only slightly more than a single time step in the fine grid.

4.8.2 Multigrid Implicit Schemes for Unsteady Flow

Time dependent calculations are needed for a number of important applications, such as flutter analysis, or the analysis of the flow past a helicopter rotor, in which the stability limit of an explicit scheme forces the use of much smaller time steps than would be needed for an accurate simulation. In this situation a multigrid explicit scheme can be used in an inner iteration to solve the equations of a fully implicit time stepping scheme [74].

Suppose that (40) is approximated as

$$D_t w^{n+1} + R(w^{n+1}) = 0.$$

Here D_t is a k^{th} order accurate backward difference operator of the form

$$D_t = \frac{1}{\Delta t} \sum_{q=1}^{k} \frac{1}{q} (\Delta^-)^q,$$

where

$$\Delta^- w^{n+1} = w^{n+1} - w^n.$$

Applied to the linear differential equation

$$\frac{dw}{dt} = \alpha w$$

the schemes with $k = 1, 2$ are stable for all $\alpha\Delta t$ in the left half plane (A-stable). Dahlquist has shown that A-stable linear multi-step schemes are at best second order accurate [38]. Gear however, has shown that the schemes with $k \leq 6$ are stiffly stable [49], and one of the higher order schemes may offer a better compromise between accuracy and stability, depending on the application.

Equation (40) is now treated as a modified steady state problem to be solved by a multigrid scheme using variable local time steps in a fictitious time t^*. For example, in the case $k = 2$ one solves

$$\frac{\partial w}{\partial t^*} = R^*(w),$$

where

$$R^*(w) = \frac{3}{2\Delta t}w + R(w) + \frac{2}{\Delta t}w^n - \frac{1}{2\Delta t}w^{n-1},$$

and the last two terms are treated as fixed source terms. The first term shifts the Fourier symbol of the equivalent model problem to the left in the complex plane. While this promotes stability, it may also require a limit to be imposed on the magnitude of the local time step Δt^* relative to that of the implicit time step Δt. This may be relieved by a point-implicit modification of the multi-stage scheme [119]. In the case of problems with moving boundaries the equations must be modified to allow for movement and deformation of the mesh.

This method has proved effective for the calculation of unsteady flows that might be associated with wing flutter [3, 4] and also in the calculation of unsteady incompressible flows [18]. It has the advantage that it can be added as an option to a computer program which uses an explicit multigrid scheme, allowing it to be used for the efficient calculation of both steady and unsteady flows.

4.9 Preconditioning

Another way to improve the rate of convergence to a steady state is to multiply the space derivatives in equation (1) by a preconditioning matrix P which is designed to equalize the eigenvalues, so that all the waves can be advanced with optimal time steps. A symmetric preconditioner which equalizes the eigenvalues has been proposed by Van Leer [102]. When the equations are written in stream-aligned coordinates this has the form

$$P = \begin{bmatrix} \frac{\tau}{\beta^2}M^2 & -\frac{\tau}{\beta}M & 0 & 0 & 0 \\ -\frac{\tau}{\beta}M & \frac{\tau}{\beta^2}+1 & 0 & 0 & 0 \\ 0 & 0 & \tau & 0 & 0 \\ 0 & 0 & 0 & \tau & 0 \\ 0 & 0 & 0 & 0 & 1 \end{bmatrix}$$

where

$$\begin{aligned} \beta &= \tau = \sqrt{1-M^2}, \quad \text{if} \quad M < 1 \\ \beta &= \sqrt{1-M^2}, \tau = \sqrt{1-\frac{1}{M^2}}, \quad \text{if} \quad M \geq 1 \end{aligned}$$

Turkel has proposed an asymmetric preconditioner which has also proved effective, particularly for flow at low Mach numbers [171]. The use of these preconditioners can lead to instability at stagnation points where there is a zero eigenvalue which cannot be equalized with the eigenvalues $\pm c$.

The preconditioners of Van Leer and Turkel do not take account of the effect of differences in the mesh intervals in the different coordinate directions. The need to resolve the boundary layer generally compels the introduction of mesh cells with very high aspect ratios near the boundary, and these can lead to a severe reduction in the rate of convergence to a steady state. Pierce has recently obtained impressive results using diagonal and block-Jacobi preconditioners which include the mesh intervals [133].

An alternative approach has recently been proposed by Ta'asan [167], in which the equations are written in a canonical form which separates the equations describing acoustic waves from those describing convection. In terms of the velocity components u, v and the vorticity ω, temperature T, entropy s and total enthalpy H, the equations describing steady two-dimensional flow can be written as

$$\begin{bmatrix} D_1 & D_2 & 0 & 0 & - \\ -\frac{\partial}{\partial y} & \frac{\partial}{\partial x} & -1 & 0 & 0 \\ 0 & 0 & -q & -\frac{c^2}{\gamma(\gamma-1)}D_3 & \frac{1}{q}D_3 \\ 0 & 0 & 0 & T\rho Q & 0 \\ 0 & 0 & 0 & 0 & \rho Q \end{bmatrix} \begin{bmatrix} u \\ v \\ \omega \\ s \\ H \end{bmatrix} = 0$$

where

$$\begin{aligned} D_1 &= \frac{\rho}{c^2}\left((c^2-u^2)\frac{\partial}{\partial x} - uv\frac{\partial}{\partial y}\right) \\ D_2 &= \frac{\rho}{c^2}\left((c^2-u^2)\frac{\partial}{\partial y} - uv\frac{\partial}{\partial x}\right) \\ D_3 &= v\frac{\partial}{\partial x} - u\frac{\partial}{\partial y} \\ Q &= u\frac{\partial}{\partial x} + v\frac{\partial}{\partial y} \end{aligned}$$

Here the first two equations describe an elliptic system if the flow is subsonic, while the remaining equations are convective. Now separately optimized multigrid procedures are used to solve the two sets of equations, which are essentially decoupled.

4.10 High Order Schemes and Mesh Refinement

The need both to improve the accuracy of computational simulations, and to assure known levels of accuracy is the focus of ongoing research. The main routes to improving the accuracy are to increase the order of the discrete scheme, and reduce the mesh interval. High order difference methods are most easily implemented on Cartesian, or at least extremely smooth grids. The expansion of the stencil as the order is increased leads to the need for complex boundary conditions. Compact schemes keep the stencil as small as possible [140, 104, 28]. On simple domains, spectral methods are particularly effective, especially in the case of periodic boundary conditions, and can be used to produce exponentially fast convergence of the error as the mesh interval is decreased [127, 27]. A compromise is to divide the field into subdomains and introduce high order elements. This approach is used in the spectral element method [92].

High order difference schemes and spectral methods have proven particularly useful in direct Navier-Stokes simulations of transient and turbulent flows. High order methods are also beneficial in computational aero-acoustics, where it is desired to track waves over long distances with minimum error. If the flow contains shock waves or contact discontinuities, the ENO method may be used to construct high order non-oscillatory schemes.

In multi-dimensional flow simulations, global reduction of the mesh interval can be prohibitively expensive, motivating the use of adaptive mesh refinement procedures which reduce the local mesh width h if there is an indication that the error is too large [21, 39, 109, 61, 138, 103]. In such h-refinement methods, simple error indicators such as local solution gradients may be used. Alternatively, the discretization error may be estimated by comparing quantities calculated with two mesh widths, say on the current mesh and a coarser mesh with double the mesh interval. Procedures of this kind may also be used to provide *a posteriori* estimates of the error once the calculation is completed.

This kind of local adaptive control can also be applied to the local order of a finite element method to produce a p-refinement method, where p represents the order of the polynomial basis functions. Finally, both h- and p- refinement can be combined to produce an h-p method in which h and p are locally optimized to yield a solution with minimum error [126]. Such methods can achieve exponentially fast convergence, and are well established in computational solid mechanics.

5 CURRENT STATUS OF NUMERICAL SIMULATION

This section presents some representative numerical results which confirm the properties of the algorithms which have been reviewed in the last section. These have been drawn from the work of the author and his associates. They also illustrate the kind of calculation which can be performed in an industrial environment, where rapid turn around is important to allow the quick assessment of design changes, and computational costs must be limited.

5.1 One dimensional shock

In order to verify the discrete structure of stationary shocks, calculations were performed for a one dimensional problem with initial data containing left and right states compatible with the Rankine Hugoniot conditions. An intermediate state consisting of the arithmetic average of the left and right states was introduced at a single cell in the center of the domain. With this intermediate state the system is not in equilibrium, and the time dependent equations were solved to find an equilibrium solution with a stationary shock wave separating the left and right states. Table 1 shows the result for a shock wave at Mach 20. This calculation used the H-CUSP scheme, which allows a solution with constant stagnation enthalpy. The SLIP-JST construction was used with the limiter defined by equation (23), and $q = 3$. The table shows the values of ρ, u, H, p, M and the entropy $S = \log \frac{p}{\rho^\gamma} - \log\left(\frac{p_L}{\rho_L^\gamma}\right)$. A perfect one point shock structure is displayed. The entropy is zero to 4 decimal places upstream of the shock, exhibits a slight excursion at the interior point, and is constant to 4 decimal places downstream of the shock. It may be noted that the mass, momentum and energy of the initial data are not compatible with the final equilibrium state. According to conservation arguements the total mass, momentum and energy must remain constant if the outflow flux f_R remains equal to the inflow flux f_L. Therefore f_R must be allowed to vary according to an appropriate outflow boundary condition to allow the total mass, momentum and energy to be adjusted to values compatible with equilibrium.

5.2 Euler Calculations for Airfoils and Wings

The results of transonic flow calculations for two well known airfoils, the RAE 2822 and the NACA

I	ρ	H	p	M
19	1.0000	283.5000	1.0000	20.0000
20	1.0000	283.5000	1.0000	20.0000
21	1.0000	283.5000	1.0000	20.0000
22	4.1924	283.4960	307.4467	0.7229
23	5.9259	283.4960	466.4889	0.3804
24	5.9259	283.4960	466.4889	0.3804
25	5.9259	283.4960	466.4889	0.3804

Table 1: Shock Wave at Mach 20

0012, are presented in figures (19-21). The H-CUSP scheme was again used with the SLIP-JST construction. The limiter defined by equation (23) was used with $q = 3$. The 5 stage time stepping scheme (42) was augmented by the multigrid scheme described in section 4.2 to accelerate convergence to a steady state. The equations were discretized on meshes with O-topology extending out to a radius of about 100 chords. In each case the calculations were performed on a sequence of successively finer meshes from 40x8 to 320x64 cells, while the multigrid cycles on each of these meshes descended to a coarsest mesh of 10x2 cells. Figures 19-21 show the final results on 320x64 meshes for the RAE 2822 airfoil at Mach .75 and 3° angle of attack, and for the NACA 0012 airfoil at Mach .8 and 1.25° angle of attack, and also at Mach .85 and 1° angle of attack. In the pressure distributions the pressure coefficient $C_p = \frac{p-p_\infty}{\frac{1}{2}\rho_\infty q_\infty^2}$ is plotted with the negative (suction) pressures upward, so that the upper curve represents the flow over the upper side of a lifting airfoil. The convergence histories show the mean rate of change of the density, and also the total number of supersonic points in the flow field, which provides a useful measure of the global convergence of transonic flow calculations such as these. In each case the convergence history is shown for 100 cycles, while the pressure distribution is displayed after a sufficient number of cycles for its convergence. The pressure distribution of the RAE 2822 airfoil converged in only 25 cycles. Convergence was slower for the NACA 0012 airfoil. In the case of flow at Mach .8 and 1.25° angle of attack, additional cycles were needed to damp out a wave downstream of the weak shock wave on the lower surface.

As a further check on accuracy the drag coefficient should be zero in subsonic flow, or in shock free transonic flow. Table 2 shows the computed drag coefficient on a sequence of three meshes for three examples. The first two are subsonic flows over the RAE 2822 and NACA 0012 airfoils at Mach .5 and 3° angle of attack. The third is the flow over the shock free Korn airfoil at its design point of Mach .75 and 0° angle of attack. In all three cases the drag coefficient is calculated to be zero to four digits on a 160x32 mesh.

Mesh	RAE 2822 Mach .50 α 3°	NACA 0012 Mach .50 α 3°	Korn Airfoil Mach .75 α 0°
40x8	.0062	.0047	.0098
80x16	.0013	.0008	.0017
160x32	.0000	.0000	.0000

Table 2: Drag Coefficient on a sequence of meshes

As a further test of the performance of the H-CUSP scheme, the flow past the ONERA M6 wing was calculated on a mesh with C-H topology and 192x32x48 = 294912 cells. Figure 22 shows the result at Mach .84 and 3.06° angle of attack. This again verifies the non-oscillatory character of the solution, and the sharp resolution of shock waves. In this case 50 cycles were sufficient for convergence of the pressure distributions.

Figure 9 shows a calculation of the Northrop YF23 by R.J. Busch, Jr., who used the author's FLO57 code to solve the Euler equations [26]. Although an inviscid model of the flow was used, it can be seen that the simulations are in good agreement with wind tunnel measurements both at Mach .90, with angles of attack of 0, 8 and 16 degrees, and at Mach 1.5 with angles of attack of 0, 4 and 8 degrees. At a high angle of attack the flow separates from the leading edge, and this example shows that in situations where the point of separation is fixed, an inviscid model may still produce a useful prediction. Thus valuable information for the aerodynamic design could be obtained with a relatively inexpensive computational model.

The next figures show the results of calculations using the AIRPLANE code developed by T.J. Baker and the author, to solve the Euler equations on an unstructured mesh. This provides the flexibility to treat arbitrarily complex configurations without the need to spend months developing an acceptable mesh. Figures 10 and 11 show calculations for supersonic transport configurations which were performed by Susan Cliff. The agreement with experimental data is quite good, and it has also been possible to predict the sonic boom signature [34]. Figure 12 shows an Euler calculation for the McDonnell Douglas MD11 with flow through the engine nacelles, using 348407 mesh points of 2100466 tetrahedra. This calculation takes 4 hours on an IBM 590 workstation. A parallel version of the code has been developed in collaboration with W.S. Chen, and the same calculation can be performed in 16 minutes using 16 processors of an IBM SP2. The parallel speed-up for the MD11 is shown in table 3.

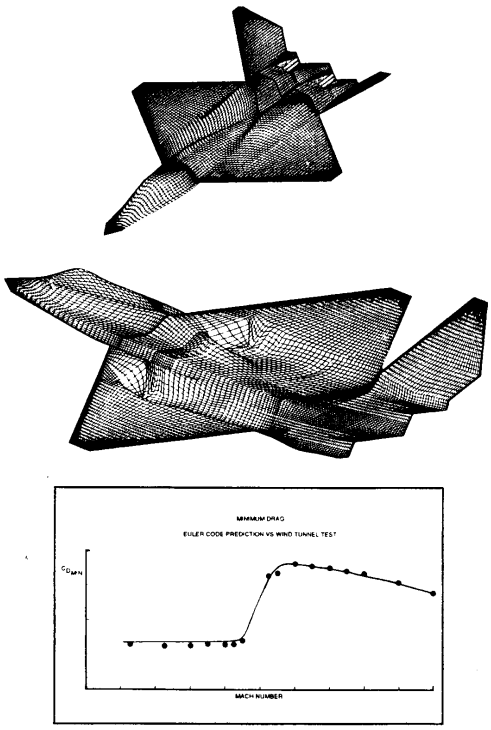

Figure 9: Comparison of Experimental and Computed Drag Rise Curve for the YF-23 (Supplied by R. J. Bush Jr.)

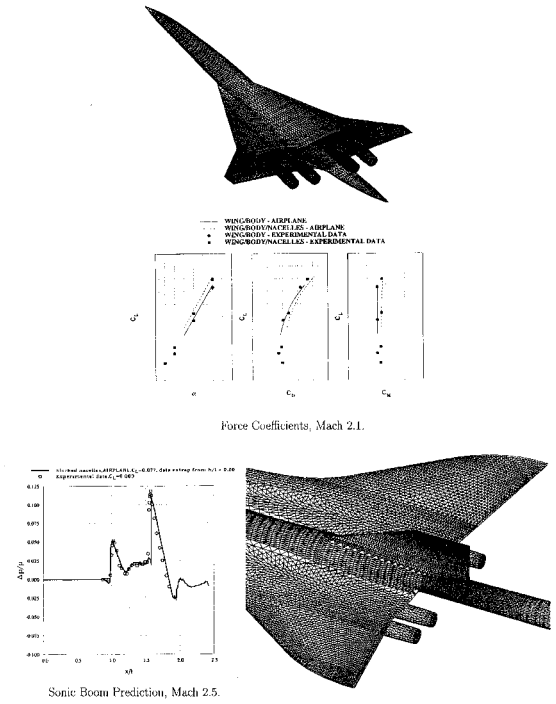

Figure 10: Comparison of Experimental and Calculated Results for a HSCT Configuration

No. of Nodes	Seconds/Cycle	Speedup
1	36.03	1.00
2	18.11	1.99
4	9.11	3.96
8	4.66	7.73
16	2.39	15.08

Table 3: AIRPLANE Parallel Performance on the SP2, MD-11 Model

5.3 Viscous Flow Calculations

The next figures show viscous simulations based on the solution of the Reynolds averaged Navier Stokes equations with turbulence models. Figure 13 shows a two-dimensional calculation for the RAE 2822 airfoil by L. Martinelli. The vertical axis represents the negative pressure coefficient, and there is a shock wave half way along the upper surface. This example confirms that in the absence of significant shock induced separation, simulations performed on a sufficiently fine mesh (512 x 64) can produce excellent agreement with experimental data. Figure 18 shows a simulation of the McDonnell-Douglas F18 performed by R.M. Cummings, Y.M. Rizk, L.B. Schiff and N.M. Chaderjian at NASA Ames [37]. They used a multiblock mesh with about 900000 mesh points. While this is probably not enough for an accurate quantitative prediction, the agreement with both the experimental data and the visualization are quite good.

Figure 14 shows an unsteady flow calculation for a pitching airfoil performed by J. Alonso using the code UFLO82, which he jointly developed with L. Martinelli and the author [4]. This uses the multigrid implicit scheme described in Section 3.7.2 which allows the number of time steps to be reduced from several thousand to 36 per pitching cycle. The agreement with experimental data is quite good.

5.4 Ship Wave Resistance calculations

Figures 51-53 show the results of an application of the same multigrid finite volume techniques to the calculation of the flow past a naval frigate, using a code which was developed by J. Farmer, L. Martinelli and the author [47]. The mesh was adjusted during the course of the calculation to conform to the free surface in order to satisfy the exact non-linear boundary condition, while artificial compressibility was used to reat the incompressible flow equations.

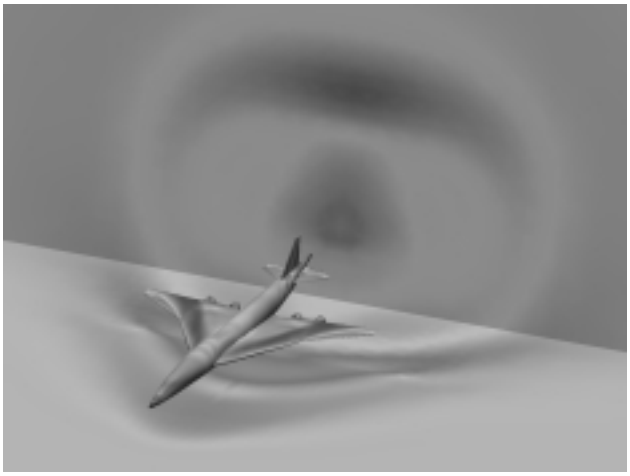

Figure 11: Pressure Contours and Sonic Boom on a Representative HSCT Configuration

Figure 12: Computed Pressure Field for a McDonnell Douglas MD11

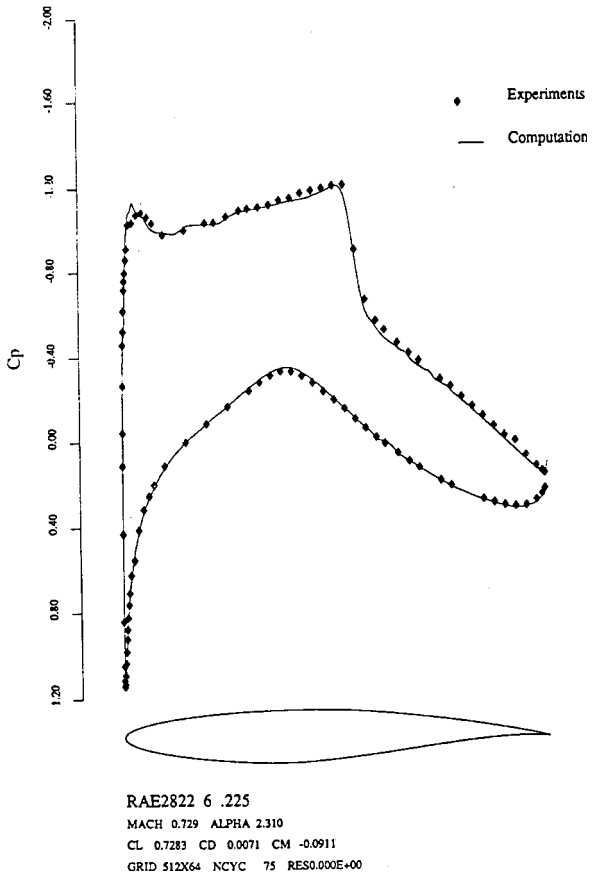

Figure 13: Two-Dimensional Turbulent Viscous Calculation (by Luigi Martinelli)

6 AERODYNAMIC SHAPE OPTIMIZATION

6.1 Optimization and Design

Traditionally the process of selecting design variations has been carried out by trial and error, relying on the intuition and experience of the designer. With currently available equipment the turn around for numerical simulations is becoming so rapid that it is feasible to examine an extremely large number of variations. It is not at all likely that repeated trials in an interactive design and analysis procedure can lead to a truly optimum design. In order to take full advantage of the possibility of examining a large design space the numerical simulations need to be combined with automatic search and optimization procedures. This can lead to automatic design methods which will fully realize the potential improvements in aerodynamic efficiency.

The simplest approach to optimization is to define the geometry through a set of design parameters, which may, for example, be the weights α_i applied to a set of shape functions $b_i(x)$ so that the shape is represented as

$$f(x) = \sum \alpha_i b_i(x).$$

Then a cost function I is selected which might, for example, be the drag coefficient or the lift to drag ratio, and I is regarded as a function of the parameters α_i. The sensitivities $\frac{\partial I}{\partial \alpha_i}$ may now be estimated by making a small variation $\delta\alpha_i$ in each design parameter in turn and recalculating the flow to obtain the change in I. Then

$$\frac{\partial I}{\partial \alpha_i} \approx \frac{I(\alpha_i + \delta\alpha_i) - I(\alpha_i)}{\delta\alpha_i}.$$

The gradient vector $\frac{\partial I}{\partial \alpha}$ may now be used to determine a direction of improvement. The simplest procedure is to make a step in the negative gradient direction by setting

$$\alpha^{n+1} = \alpha^n - \lambda\delta\alpha,$$

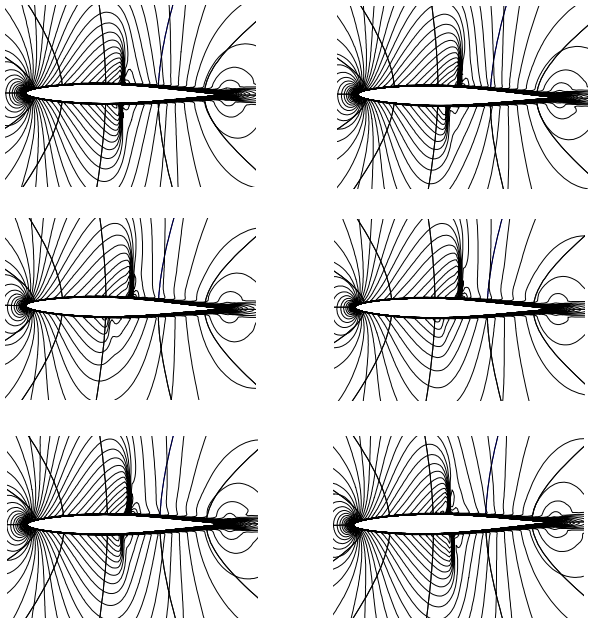

Figure 14: Mach Number Contours. Pitching Airfoil Case. $Re = 1.0 \times 10^6$, $M_\infty = 0.796$, $K_c = 0.202$.

so that to first order

$$I + \delta I = I - \frac{\partial I^T}{\partial \alpha}\delta\alpha = I - \lambda \frac{\partial I^T}{\partial \alpha}\frac{\partial I}{\partial \alpha}.$$

More sophisticated search procedures may be used such as quasi-Newton methods, which attempt to estimate the second derivative $\frac{\partial^2 I}{\partial \alpha_i \partial \alpha_j}$ of the cost function from changes in the gradient $\frac{\partial I}{\partial \alpha}$ in successive optimization steps. These methods also generally introduce line searches to find the minimum in the search direction which is defined at each step. The main disadvantage of this approach is the need for a number of flow calculations proportional to the number of design variables to estimate the gradient. The computational costs can thus become prohibitive as the number of design variables is increased.

An alternative approach is to cast the design problem as a search for the shape that will generate the desired pressure distribution. This approach recognizes that the designer usually has an idea of the the kind of pressure distribution that will lead to the desired performance. Thus, it is useful to consider the inverse problem of calculating the shape that will lead to a given pressure distribution. The method has the advantage that only one flow solution is required to obtain the desired design. Unfortunately, a physically realizable shape may not necessarily exist, unless the pressure distribution satisfies certain constraints. Thus the problem must be very carefully formulated; otherwise it may be ill posed.

The difficulty that the target pressure may be unattainable may be circumvented by treating the inverse problem as a special case of the optimization problem, with a cost function which measures the error in the solution of the inverse problem. For example, if p_d is the desired surface pressure, one may take the cost function to be an integral over the the body surface of the square of the pressure error,

$$I = \frac{1}{2}\int_{\mathcal{B}} (p - p_d)^2 d\mathcal{B},$$

or possibly a more general Sobolev norm of the pressure error. This has the advantage of converting a possibly ill posed problem into a well posed one. It has the disadvantage that it incurs the computational costs associated with optimization procedures.

6.2 Application of Control Theory

In order to reduce the computational costs, it turns out that there are advantages in formulating both the inverse problem and more general aerodynamic problems within the framework of the mathematical theory for the control of systems governed by partial differential equations [105]. A wing, for example, is a device to produce lift by controlling the flow, and its design can be regarded as a problem in the optimal control of the flow equations by variation of the shape of the boundary. If the boundary shape is regarded as arbitrary within some requirements of smoothness, then the full generality of shapes cannot be defined with a finite number of parameters, and one must use the concept of the Frechet derivative of the cost with respect to a function. Clearly, such a derivative cannot be determined directly by finite differences of the design parameters because there are now an infinite number of these. Using techniques of control theory, however, the gradient can be determined indirectly by solving an adjoint equation which has coefficients defined by the solution of the flow equations. The cost of solving the adjoint equation is comparable to that of solving the flow equations. Thus the gradient can be determined with roughly the computational costs of two flow solutions, independently of the number of design variables, which may be infinite if the boundary is regarded as a free surface.

For flow about an airfoil or wing, the aerodynamic properties which define the cost function are functions of the flow-field variables (w) and the physical location of the boundary, which may be represented by the function $\mathcal{F}$, say. Then

$$I = I\left(w, \mathcal{F}\right),$$

and a change in $\mathcal{F}$ results in a change

$$\delta I = \frac{\partial I^T}{\partial w}\delta w + \frac{\partial I^T}{\partial \mathcal{F}}\delta\mathcal{F}, \tag{43}$$

in the cost function. Using control theory, the governing equations of the flowfield are introduced as a constraint in such a way that the final expression for the gradient does not require reevaluation of the flowfield. In order to achieve this δw must be eliminated from (43). Suppose that the governing equation R which expresses the dependence of w and $\mathcal{F}$ within the flowfield domain D can be written as

$$R\left(w,\mathcal{F}\right)=0. \tag{44}$$

Then δw is determined from the equation

$$\delta R=\left[\frac{\partial R}{\partial w}\right]\delta w+\left[\frac{\partial R}{\partial \mathcal{F}}\right]\delta\mathcal{F}=0. \tag{45}$$

Next, introducing a Lagrange Multiplier ψ, we have

$$\begin{aligned}\delta I &= \frac{\partial I^T}{\partial w}\delta w+\frac{\partial I^T}{\partial \mathcal{F}}\delta\mathcal{F}-\psi^T\left(\left[\frac{\partial R}{\partial w}\right]\delta w+\left[\frac{\partial R}{\partial \mathcal{F}}\right]\delta\mathcal{F}\right)\\ &= \left\{\frac{\partial I^T}{\partial w}-\psi^T\left[\frac{\partial R}{\partial w}\right]\right\}\delta w+\left\{\frac{\partial I^T}{\partial \mathcal{F}}-\psi^T\left[\frac{\partial R}{\partial \mathcal{F}}\right]\right\}\delta\mathcal{F}.\end{aligned}$$

Choosing ψ to satisfy the adjoint equation

$$\left[\frac{\partial R}{\partial w}\right]^T\psi=\frac{\partial I}{\partial w} \tag{46}$$

the first term is eliminated, and we find that

$$\delta I=\mathcal{G}\delta\mathcal{F}, \tag{47}$$

where

$$\mathcal{G}=\frac{\partial I^T}{\partial \mathcal{F}}-\psi^T\left[\frac{\partial R}{\partial \mathcal{F}}\right].$$

The advantage is that (47) is independent of δw, with the result that the gradient of I with respect to an arbitrary number of design variables can be determined without the need for additional flow-field evaluations. In the case that (44) is a partial differential equation, the adjoint equation (46) is also a partial differential equation and appropriate boundary conditions must be determined.

After making a step in the negative gradient direction, the gradient can be recalculated and the process repeated to follow a path of steepest descent until a minimum is reached. In order to avoid violating constraints, such as a minimum acceptable wing thickness, the gradient may be projected into the allowable subspace within which the constraints are satisfied. In this way one can devise procedures which must necessarily converge at least to a local minimum, and which can be accelerated by the use of more sophisticated descent methods such as conjugate gradient or quasi-Newton algorithms. There is the possibility of more than one local minimum, but in any case the method will lead to an improvement over the original design. Furthermore, unlike the traditional inverse algorithms, any measure of performance can be used as the cost function.

In reference [72] the author derived the adjoint equations for transonic flows modelled by both the potential flow equation and the Euler equations. The theory was developed in terms of partial differential equations, leading to an adjoint partial differential equation. In order to obtain numerical solutions both the flow and the adjoint equations must be discretized. The control theory might be applied directly to the discrete flow equations which result from the numerical approximation of the flow equations by finite element, finite volume or finite difference procedures. This leads directly to a set of discrete adjoint equations with a matrix which is the transpose of the Jacobian matrix of the full set of discrete nonlinear flow equations. On a three-dimensional mesh with indices i,j,k the individual adjoint equations may be derived by collecting together all the terms multiplied by the variation $\delta w_{i,j,k}$ of the discrete flow variable $w_{i,j,k}$. The resulting discrete adjoint equations represent a possible discretization of the adjoint partial differential equation. If these equations are solved exactly they can provide an exact gradient of the inexact cost function which results from the discretization of the flow equations. On the other hand any consistent discretization of the adjoint partial differential equation will yield the exact gradient in the limit as the mesh is refined. The trade-off between the complexity of the adjoint discretization, the accuracy of the resulting estimate of the gradient, and its impact on the computational cost to approach an optimum solution is a subject of ongoing research, as indeed also remains true for the discretization of the flow equations.

The true optimum shape belongs to an infinitely dimensional space of design parameters. One motivation for developing the theory for the partial differential equations of the flow is to provide an indication in principle of how such a solution could be approached if sufficient computational resources were available. Another motivation is that it highlights the possibility of generating ill posed formulations of the problem. For example, if one attempts to calculate the sensitivity of the pressure at a particular location to changes in the boundary shape, there is the possibility that a shape modification could cause a shock wave to pass over that location. Then the sensitivity could become unbounded. The movement of the shock, however, is continuous as the shape changes. Therefore a quantity such as the drag coefficient, which is determined by integrating the pressure over the surface, also depends continuously on the shape. The adjoint equation allows the sensitivity of the drag coefficient to be determined without the explicit evaluation of pressure sensitivities which would be ill posed.

The discrete adjoint equations, whether they are de-

rived directly or by discretization of the adjoint partial differential equation, are linear. Therefore they could be solved by direct numerical inversion. In three-dimensional problems on a mesh with, say, n intervals in each coordinate direction, the number of unknowns is proportional to n^3 and the bandwidth to n^2. The complexity of direct inversion is proportional to the number of unknowns multiplied by the square of the bandwidth, resulting in a complexity proportional to n^7. The cost of direct inversion can thus become prohibitive as the mesh is refined, and it becomes more efficient to use iterative solution methods. Moreover, because of the similarity of the adjoint equations to the flow equations, the same iterative methods which have been proved to be efficient for the solution of the flow equations are efficient for the solution of the adjoint equations.

The control theory formulation for optimal aerodynamic design has proved effective in a variety of applications [73, 77, 142]. The adjoint equations have also been used by Ta'asan, Kuruvila and Salas [166], who have implemented a one shot approach in which the constraint represented by the flow equations is only required to be satisfied by the final converged solution, and computational costs are also reduced by applying multigrid techniques to the geometry modifications as well as the solution of the flow and adjoint equations. Pironneau has studied the use of control theory for optimal shape design of systems governed by elliptic equations [134], and more recently the Navier-Stokes equations, and also wave reflection problems. Adjoint methods have also been used by Baysal and Eleshaky [16].

6.3 Three-Dimensional Design using the Euler Equations

In order to illustrate the application of control theory to aerodynamic design problems, this section treats the case of three-dimensional wing design using the inviscid Euler equations as the mathematical model for compressible flow. A transformation to a body-fitted coordinate system will be introduced, so that variations in the wing shape induce corresponding variations in the computational mesh. Thus the flow is determined by the solution of the transformed equation (5). Let

$$K_{ij} = \left[\frac{\partial x_i}{\partial \xi_j}\right], J = \det(K), K^{-1}_{ij} = \left[\frac{\partial \xi_i}{\partial x_j}\right],$$

and

$$Q = JK^{-1}.$$

The elements of Q are the coefficients of K, and in a finite volume discretization they are just the face areas of the computational cells projected in the x_1, x_2, and x_3 directions. Also introduce scaled contravariant velocity components

$$U_i = Q_{ij}u_j.$$

The transformed equations can now be written as

$$\frac{\partial W}{\partial t} + \frac{\partial F_i}{\partial \xi_i} = 0 \tag{48}$$

where

$$W = Jw$$

and

$$F_i = Q_{ij}f_j = \begin{bmatrix} \rho U_i \\ \rho U_i u_1 + Q_{i1}p \\ \rho U_i u_2 + Q_{i2}p \\ \rho U_i u_3 + Q_{i3}p \\ \rho U_i H \end{bmatrix}$$

Assume now that the new computational coordinate system conforms to the wing in such a way that the wing surface B_W is represented by $\xi_2 = 0$. Then the flow is determined as the steady state solution of equation (48) subject to the flow tangency condition

$$U_2 = 0 \quad \text{on } B_W. \tag{49}$$

At the far field boundary B_F, conditions are specified for incoming waves, as in the two-dimensional case, while outgoing waves are determined by the solution.

The weak form of the Euler equations for steady flow can be written as

$$\int_{\mathcal{D}} \frac{\partial \phi^T}{\partial \xi_i} F_i d\mathcal{D} = \int_{\mathcal{B}} n_i \phi^T F_i d\mathcal{B}, \tag{50}$$

where the test vector ϕ is an arbitrary differentiable function and n_i is the outward normal at the boundary. If a differentiable solution w is obtained to this equation, it can be integrated by parts to give

$$\int_{\mathcal{D}} \phi^T \frac{\partial F_i}{\partial \xi_i} d\mathcal{D} = 0$$

and since this is true for any ϕ, the differential form can be recovered. If the solution is discontinuous, equation (50) may be integrated by parts separately on either side of the discontinuity to recover the shock jump conditions.

Suppose now that it is desired to control the surface pressure by varying the wing shape. It is convenient to retain a fixed computational domain. Variations in the shape then result in corresponding variations in the mapping derivatives defined by K. Introduce the cost function

$$I = \frac{1}{2}\iint_{B_W} (p - p_d)^2 \, d\xi_1 d\xi_3,$$

where p_d is the desired pressure. The design problem is now treated as a control problem where the control

function is the wing shape, which is to be chosen to minimize I subject to the constraints defined by the flow equations (48–50). A variation in the shape will cause a variation δp in the pressure and consequently a variation in the cost function

$$\delta I = \iint_{B_W} (p - p_d)\, \delta p \;\; d\xi_1 d\xi_3. \tag{51}$$

Since p depends on w through the equation of state (2), the variation δp can be determined from the variation δw. Define the Jacobian matrices

$$A_i = \frac{\partial f_i}{\partial w}, \quad C_i = Q_{ij} A_j. \tag{52}$$

The weak form of the equation for δw in the steady state becomes

$$\int_{\mathcal{D}} \frac{\partial \phi^T}{\partial \xi_i} \delta F_i d\mathcal{D} = \int_{\mathcal{B}} (n_i \phi^T \delta F_i) d\mathcal{B},$$

where

$$\delta F_i = C_i \delta w + \delta Q_{ij} f_j,$$

which should hold for any differential test function ϕ. This equation may be added to the variation in the cost function, which may now be written as

$$\begin{aligned} \delta I = & \iint_{B_W} (p - p_d)\, \delta p \;\; d\xi_1 d\xi_3 \\ & - \int_{\mathcal{D}} \left(\frac{\partial \psi^T}{\partial \xi_i} \delta F_i \right) d\mathcal{D} \\ & + \int_{\mathcal{B}} \left(n_i \psi^T \delta F_i \right) d\mathcal{B}. \end{aligned} \tag{53}$$

On the wing surface B_W, $n_1 = n_3 = 0$ and it follows from equation (49) that

$$\delta F_2 = \begin{bmatrix} 0 \\ Q_{21}\delta p \\ Q_{22}\delta p \\ Q_{23}\delta p \\ 0 \end{bmatrix} + \begin{bmatrix} 0 \\ \delta Q_{21} p \\ \delta Q_{22} p \\ \delta Q_{23} p \\ 0 \end{bmatrix}. \tag{54}$$

Since the weak equation for δw should hold for an arbitrary choice of the test vector ϕ, we are free to choose ϕ to simplify the resulting expressions. Therefore we set $\phi = \psi$, where the costate vector ψ is the solution of the adjoint equation

$$\frac{\partial \psi}{\partial t} - C_i^T \frac{\partial \psi}{\partial \xi_i} = 0 \quad \text{in } D. \tag{55}$$

At the outer boundary incoming characteristics for ψ correspond to outgoing characteristics for δw. Consequently one can choose boundary conditions for ψ such that

$$n_i \psi^T C_i \delta w = 0.$$

Then if the coordinate transformation is such that δQ is negligible in the far field, the only remaining boundary term is

$$-\iint_{B_W} \psi^T \delta F_2 \; d\xi_1 d\xi_3.$$

Thus by letting ψ satisfy the boundary condition,

$$Q_{21}\psi_2 + Q_{22}\psi_3 + Q_{23}\psi_4 = (p - p_d) \;\; \text{on } B_W, \tag{56}$$

we find finally that

$$\begin{aligned} \delta I \;\; = & - \int_{\mathcal{D}} \frac{\partial \psi^T}{\partial \xi_i} \delta Q_{ij} f_j d\mathcal{D} \\ & - \iint_{B_W} (\delta Q_{21}\psi_2 + \delta Q_{22}\psi_3 + Q_{23}\psi_4)\, p\, d\xi_1 d\xi_3. \end{aligned} \tag{57}$$

A convenient way to treat a wing is to introduce

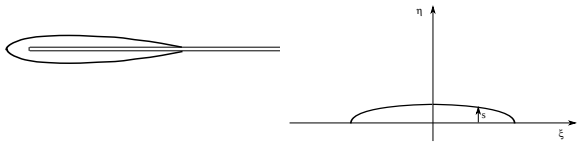

15a: x, y-Plane. 15b: ξ, η-Plane.

Figure 15: Sheared Parabolic Mapping.

sheared parabolic coordinates as shown in figure 15 through the transformation

$$\begin{aligned} x &= x_0(\zeta) + \frac{1}{2} a(\zeta) \left\{ \xi^2 - (\eta + \mathcal{S}(\xi, \zeta))^2 \right\} \\ y &= y_0(\zeta) + a(\zeta)\, \xi\, (\eta + \mathcal{S}(\xi, \zeta)) \\ z &= \zeta. \end{aligned}$$

Here $x = x_1$, $y = x_2$, $z = x_3$ are the Cartesian coordinates, and ξ and $\eta + \mathcal{S}$ correspond to parabolic coordinates generated by the mapping

$$x + iy = x_0 + iy_0 + \frac{1}{2} a(\zeta) \{\xi + i(\eta + \mathcal{S})\}^2$$

at a fixed span station ζ. $x_0(\zeta)$ and $y_0(\zeta)$ are the coordinates of a singular line which is swept to lie just inside the leading edge of a swept wing, while $a(\zeta)$ is a scale factor to allow for spanwise chord variations.

We now treat $\mathcal{S}(\xi, \zeta)$ as the control. Substitution of these formulas yields the variation in the form

$$\delta I = \int \int \mathcal{G}(\xi, \eta) \delta S(\xi, \eta) d\xi d\eta$$

where the gradient $\mathcal{G}(\xi, \eta)$ is obtained by evaluating the integrals in equation (57). Thus to reduce I we can choose

$$\delta \mathcal{S} = -\lambda \mathcal{G}$$

where λ is sufficiently small and non-negative. In order to impose a thickness constraint we can define

a baseline surface $\mathcal{S}_0(\xi,\zeta)$ below which $\mathcal{S}(\xi,\zeta)$ is not allowed to fall. Now we take $\lambda = \lambda(\xi,\zeta)$ as a non-negative function such that

$$\mathcal{S}(\xi,\zeta) + \delta\mathcal{S}(\xi,\zeta) \geq \mathcal{S}_0(\xi,\zeta). \tag{58}$$

Then the constraint is satisfied, while

$$\delta I = -\iint_{B_W} \lambda \mathcal{G}^2 d\xi\, d\zeta \leq 0.$$

The costate solution ψ is a legitimate test function for the weak form of the flow equations only if it is differentiable. Smoothness should also be preserved in the redesigned shape. It is therefore crucially important to introduce appropriate smoothing procedures. In order to avoid discontinuities in the adjoint boundary condition which would be caused by the appearance of shock waves, the cost function for the target pressure may be modified to the form

$$\begin{aligned} I &= \frac{1}{2}\iint \left(\lambda_1 \mathcal{Z} + \lambda_2 \left(\frac{\partial \mathcal{Z}}{\partial \xi}\right)^2\right) d\xi d\eta \\ \lambda_1 \mathcal{Z} &- \frac{\partial}{\partial \xi}\lambda_2 \frac{\partial \mathcal{Z}}{\partial \xi} = p - p_d. \end{aligned}$$

Then

$$\begin{aligned} \delta I &= \iint \left(\lambda_1 \mathcal{Z}\delta\mathcal{Z} + \lambda_2 \frac{\partial \mathcal{Z}}{\partial \xi}\frac{\partial}{\partial \xi}\delta\mathcal{Z}\right) d\xi d\eta \\ &= \iint \mathcal{Z}\left(\lambda_1 - \frac{\partial}{\partial \xi}\lambda_2 \frac{\partial}{\partial \xi}\right)\delta\mathcal{Z}\, d\xi d\eta \\ &= \iint \mathcal{Z}\delta p\, d\xi d\eta \end{aligned}$$

and the smooth quantity $\mathcal{Z}$ replaces $p - p_d$ in the adjoint boundary condition.

Independent movement of the boundary mesh points could produce discontinuities in the designed shape. In order to prevent this the gradient may be also smoothed. Both explicit and implicit smoothing procedures are useful. Suppose that the movement of the surface mesh points were defined by local B-splines. In the case of a uniform one-dimensional mesh, a B-spline with a displacement d centered at the mesh point i would produce displacements $d/4$ at $i+1$ and $i-1$ and zero elsewhere, while preserving continuity of the first and second derivatives. Thus we can suppose that the discrete surface displacement has the form

$$\delta S = Bd,$$

where B is a matrix with coefficients defined by the B-splines, and d_i is the displacement associated with the B-spline centered at i. Then, using the discrete formulas, to first order the change in the cost is

$$\delta I = \mathcal{G}^T \delta S = \mathcal{G}^T B d.$$

Thus the gradient with respect to the B-spline coefficients is obtained by multiplying $\mathcal{G}$ by B^T, and a descent step is defined by setting

$$d = -\lambda B^T \mathcal{G},\ \delta S = Bd = -\lambda B B^T \mathcal{G}$$

where λ is sufficiently small and positive. The coefficients of B can be renormalized to produce unit row sums. With a uniform mesh spacing in the computational domain this formula is equivalent to the use of a gradient modified by two passes of the explicit smoothing procedure

$$\bar{\mathcal{G}}_{i,k} = \frac{1}{6}\mathcal{G}_{i-1,k} + \frac{2}{3}\mathcal{G}_{i,k} + \frac{1}{6}\mathcal{G}_{i+1,k}$$

with a similar smoothing procedure in the k discretization.

Implicit smoothing may also be used. The smoothing equation

$$-\epsilon_{i+\frac{1}{2},k}(\bar{\mathcal{G}}_{i+1,k} - \bar{\mathcal{G}}_{i,k}) + \epsilon_{i-\frac{1}{2},k}(\bar{\mathcal{G}}_{i,k} - \bar{\mathcal{G}}_{i-1,k}) = \mathcal{G}_{i,k}$$

approximates the differential equation

$$\bar{\mathcal{G}} - \frac{\partial}{\partial \xi}\epsilon \frac{\partial \bar{\mathcal{G}}}{\partial \xi} = \mathcal{G}$$

If one sets $\delta S = -\lambda \bar{\mathcal{G}}$, then to first order the change in the cost is

$$\begin{aligned} \delta I &= -\iint \mathcal{G}\delta S\, d\xi d\eta \\ &= -\frac{1}{\lambda}\iint \left(\bar{\mathcal{G}} - \frac{\partial}{\partial \xi}\epsilon\frac{\partial \bar{\mathcal{G}}}{\partial \xi}\right)\bar{\mathcal{G}}\, d\xi d\eta \\ &= -\frac{1}{\lambda}\iint \left(\bar{\mathcal{G}}^2 + \epsilon\left(\frac{\partial \bar{\mathcal{G}}}{\partial \xi}\right)^2\right) d\xi d\eta \\ &< 0, \end{aligned}$$

assuring an improvement if λ is sufficiently small and positive, unless the process has already reached a stationary point at which $\mathcal{G} = 0$.

6.4 Design of Swept Wings for Very Low Shock Drag

The method has been used to carry out a study of swept wing designs which might be appropriate for long range transport aircraft. Since three dimensional calculations require substantial computational resources, it is extremely important for the practical implementation of the method to use fast solution algorithms for the flow and the adjoint equations. In this case the author's FLO87 computer program has been used as the basis of the design method. FLO87 solves the three dimensional Euler equations with a cell-centered finite volume scheme, and uses residual averaging and multigrid acceleration to obtain

very rapid steady state solutions, usually in 25 to 50 multigrid cycles [66, 70]. Upwind biasing is used to produce non-oscillatory solutions, and assure the clean capture of shock waves. This is introduced through the addition of carefully controlled numerical diffusion terms, with a magnitude of order Δx^3 in smooth parts of the flow. The adjoint equations are treated in the same way as the flow equations. The fluxes are first estimated by central differences, and then modified by downwind biasing through numerical diffusive terms which are supplied by the same subroutines that were used for the flow equations.

The study has been focussed on wings designed for cruising at Mach .85, with lift coefficients in the range of .5 to .55. In every case, the wing planform was fixed while the sections were free to be changed arbitrarily by the design method, with a restriction on the minimum thickness. The initial wing has a unit-semi-span, with 38 degrees leading edge sweep. It has a modified trapezoidal planform, with straight taper from a root chord of 0.38, and a curved trailing edge in the inboard region blending into straight taper outboard of the 30 percent span station to a tip chord of 0.10, with an aspect ratio of 9.0. The initial wing sections were based on a section specifically designed by the author's two dimensional design method [73] to give shock free flow at Mach 0.78 with a lift coefficient of 0.6. This section, which has a thickness to chord ratio of 9.5 percent, was used at the tip. Similar sections with an increased thickness were used inboard. The variation of thickness was non-linear with a more rapid increase near the root, where the thickness to chord ratio of the basic section was multiplied by a factor of 1.47. The inboard sections were rotated upwards to give the initial wing 3.5 degrees twist from root to tip. The two-dimensional pressure distribution of the basic wing section at its design point was introduced as a target pressure distribution uniformly across the span. This target is presumably not realizable, but serves to favor the establishment of a relatively benign pressure distribution. The total inviscid drag coefficient, due to the combination of vortex and shock wave drag, was also included in the cost function. Since the main objective of the study was to minimize the drag, the target pressure distribution was reset after every fourth design cycle to a distribution derived by smoothing the existing pressure distribution. This allows the scheme more freedom to make changes which reduce drag. The calculations were performed with the lift coefficient forced to approach a fixed value by adjusting the angle of attack every fifth iteration of the flow solution. It was found that the computational costs can be reduced by using only 15 multigrid cycles in each flow solution, and in each adjoint solution. Although this is not enough for full convergence, it proves sufficient to provide a shape modification which leads to an improvement.

Figures 23 and 24 show a wing which was designed for a lift coefficient of .50 at Mach .85. In order to prevent the final wing from becoming too thin the threshold $\mathcal{S}_0(\xi,\eta)$ was set at three quarters of the height of the bump $\mathcal{S}(\xi,\eta)$ defining the initial wing. This calculation was performed on a mesh with 192 intervals in the ξ direction wrapping around the wing, 32 intervals in the normal η direction and 48 intervals in the spanwise ζ direction, giving a total of 294912 cells. The wing was specified by 33 sections, each with 128 points, giving a total of 4224 design variables. The plots show the initial wing geometry and pressure distribution, and the modified geometry and pressure distribution after 40 design cycles. The total inviscid drag coefficient was reduced from 0.0210 to 0.0112. The initial design exhibits a very strong shock wave in the inboard region. It can be seen that this is completely eliminated, leaving a very weak shock wave in the outboard region. To verify the solution, the final geometry was analyzed with another method, using the computer program FLO67. This program uses a cell-vertex formulation, and has recently been modified to incorporate a local extremum diminishing algorithm with a very low level of numerical diffusion [76]. When run to full convergence it was found that a better estimate of the drag coefficient of the redesigned wing is 0.0094 at Mach 0.85 with a lift coefficient of 0.5, giving a lift to drag ratio of 53. The results from FLO67 for the initial and final wings are illustrated in Figures 25 and 26. A calculation at Mach 0.500 shows a drag coefficient of 0.0087 for a lift coefficient of 0.5. Since in this case the flow is entirely subsonic, this provides an estimate of the vortex drag for this planform and lift distribution, which is just what one obtains from the standard formula for induced drag, $C_D = {C_L}^2/\epsilon\pi AR$, with an aspect ratio $AR = 9$, and an efficiency factor $\epsilon = 0.97$. Thus the design method has reduced the shock wave drag coefficient to about 0.0007 at a lift coefficient of 0.5. Figure 27 shows the result of an analysis for an off design point with the Mach number increased to .86 with the same lift coefficient of .5. This results in a flat-topped pressure distribution terminating with a weak shock of nearly uniform strength across the whole span. The drag coefficient is .0097. The penalty of .0003 is so small that this might be a preferred cruising condition.

A second wing was designed in exactly the same manner as the first, starting from the same initial geometry and with the same constraints, to give a lift coefficient of .55 at Mach .85. This produces stronger shock waves and is therefore a more severe test of the method. In this case the total inviscid drag coefficient was reduced from 0.0243 to 0.0134

in 40 design cycles. Again the performance of the final design was verified by a calculation with FLO67, and when the result was fully converged the drag coefficient was found to be 0.0115. A subsonic calculation at Mach .500 shows a drag coefficient of 0.0107 for a lift coefficient of 0.55. Thus in this case the shock wave drag coefficient is about 0.0008. For a representative transport aircraft the parasite drag coefficient of the wing due to skin friction is about 0.0045. Also the fuselage drag coefficient is about 0.0050, the nacelle drag coefficient is about 0.0015, the empennage drag coefficient is about 0.0020, and excrescence drag coefficient is about 0.0010. This would give a total drag coefficient $C_D = 0.0255$ for a lift coefficient of 0.55, corresponding to a lift to drag ratio $L/D = 21.6$. This would be a substantial improvement over the values obtained by currently flying transport aircraft.

6.5 Optimization of Complex Configurations

In order to treat more complex configurations one can use a numerical grid generation procedure to produce a body-fitted mesh for the initial geometry, and then modify the mesh in subsequent design cycles by an analytic perturbation formula. In the two-dimensional case, for example, with computational coordinates ξ, η, let the boundary displacement at $\eta = 0$ be $\delta x_b(\xi)$, $\delta y_b(\xi)$. Then the mesh points along the radial coordinate lines $\xi =$ constant can be replaced by

$$\begin{aligned} \delta x(\xi,\eta) &= \mathcal{R}(\eta)\delta x_b(\xi) \\ \delta y(\xi,\eta) &= \mathcal{R}(\eta)\delta y_b(\xi) \end{aligned}$$

yielding

$$\delta K = \begin{bmatrix} \mathcal{R}(\eta)\frac{\partial}{\partial\xi}\delta x_b & \frac{d\mathcal{R}}{d\eta}\delta x_b \\ \mathcal{R}(\eta)\frac{\partial}{\partial\xi}\delta y_b & \frac{d\mathcal{R}}{d\eta}\delta y_b \end{bmatrix}$$

Such a procedure has been implemented by J. Reuther for the three-dimensional Euler equations, and applied to the optimization of wing-body configurations [143].

It is also possible to show that in the continuous limit the field integral in equation (57) can be eliminated. Let the change in the coordinates x_i at fixed ξ be $\delta x_i(\xi)$. Then, using the fact that the fluxes $f_j(w)$ satisfy the flow equation (48), it is possible to show by a direct calculation that

$$\frac{\partial}{\partial\xi_i}\delta Q_{ij} f_j = \frac{\partial}{\partial\xi_i} Q_{ij} \frac{\partial f_j}{\partial w}\frac{\partial w}{\partial\xi_k}\delta\xi_k$$

where

$$\delta\xi = K^{-1}\delta x.$$

A detailed derivation is given in reference [78]. Thus the perturbation equation can be written as

$$\frac{\partial}{\partial\xi_i}\left\{\frac{\partial f_j}{\partial w}\left(\delta w + \delta w^*\right)\right\} = 0$$

where δw is the variation in the solution at fixed ξ caused by the change in the boundary, while δw^* is the change in the original solution $w(\xi)$ corresponding to the mesh movement $\delta x(\xi)$

$$\delta w_i^* = \frac{\partial w_i}{\partial\xi_k}\delta\xi_k$$

Now

$$\begin{aligned} \int \psi^T \frac{\partial}{\partial\xi_i}\delta F_i d\xi &= \int_{\mathcal{B}} n_i \psi^T \delta F_i d\xi_{\mathcal{B}} \\ &- \int_{\mathcal{D}} \frac{\partial\psi^T}{\partial\xi_i} C_i(\delta w + \delta w^*) d\xi \end{aligned}$$

and if ψ satisfies the adjoint equation the entire field integral is eliminated, leaving only the boundary integral in equation (57).

In an actual discretization the field terms are not zero, but this result suggests that they should be small is a fine enough mesh is used, and might be dropped. This allows a drastic simplification of the treatment of complex configurations. Preliminary numerical experiments with airfoil and wing calculations indicate roughly the same convergence with and without the field terms in the gradient.

7 OUTLOOK AND CONCLUSIONS

Better algorithms and better computer hardware have contributed about equally to the progress of computational science in the last two decades. In 1970 the Control Data 6600 represented the state of the art in computer hardware with a speed of about 10^6 operations per second (one megaflop), while in 1990 the 8 processor Cray YMP offered a performance of about 10^9 operations per second (one gigaflop). Correspondingly, steady-state Euler calculations which required 5,000–10,000 steps prior to 1980 could be performed in 10–50 steps in 1990 using multigrid acceleration. With the advent of massively parallel computers it appears that the progress of computer hardware may even accelerate. Teraflop machines offering further improvement by a factor of 1,000 are likely to be available within a few years. Parallel architectures will force a reappraisal of existing algorithms, and their effective utilization will require the extensive development of new parallel software.

In parallel with the transition to more sophisticated algorithms, the present challenge is to extend the effective use of CFD to more complex applications. A key problem is the treatment of multiple space and time scales. These arise not only in turbulent flows, but also in many other situations such as chemically reacting flows, combustion, flame fronts and plasma dynamics. Another challenge, is presented by problems with moving boundaries. Examples include helicopter rotors, and rotor-stator interaction in turbomachinery. Algorithms for these problems can be significantly improved by innovative concepts, such as the idea of time inclining. It can be anticipated that interdisciplinary applications in which CFD is coupled with the computational analysis of other properties of the design will play an increasingly important role. These applications may include structural, thermal and electromagnetic analysis. Aeroelastic problems and integrated control system and aerodynamic design are likely target areas. The

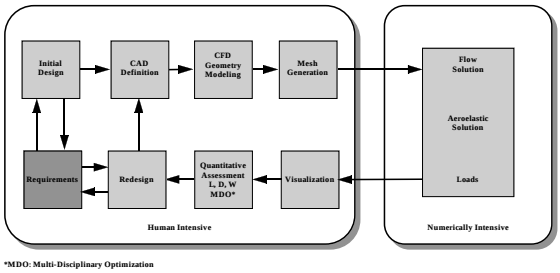

Figure 16: Concept for a numerical wind tunnel.

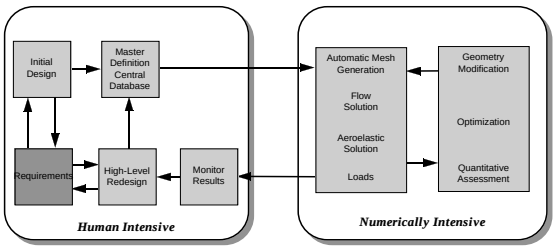

Figure 17: Advanced numerical wind tunnel.

development of improved algorithms continues to be important in providing the basic building blocks for numerical simulation. In particular, better error estimation procedures must be developed and incorporated in the simulation software to provide error control. The basic simulation software is only one of the needed ingredients, however. The flow solver must be embedded in a user-friendly system for geometry modeling, output analysis, and data management that will provide a complete numerical design environment. These are the ingredients which are needed for the full realization of the concept of a numerical wind tunnel. Figures 16 and 17 illustrate the way in which a numerical wind tunnel might evolve from current techniques, which involve massive data handling tasks, to a fully integrated design environment.

In the long run, computational simulation should become the principal tool of the aerodynamic design process because of the flexibility it provides for the rapid and comparatively inexpensive evaluation of alternative designs, and because it can be integrated in a numerical design environment providing for both multi-disciplinary analysis and multi-disciplinary optimization.

REFERENCES

[1] R. Abid, C.G. Speziale, and S. Thangam. Application of a new k-τ model to near wall turbulent flows. AIAA Paper 91-0614, AIAA 29th Aerospace Sciences Meeting, Reno, NV, January 1991.

[2] H. Aiso. Admissibility of difference approximations for scalar conservation laws. *Hiroshima Math. Journal*, 23:15–61, 1993.

[3] J. J. Alonso and A. Jameson. Fully-implicit time-marching aeroelastic solutions. *AIAA paper 94-0056*, AIAA 32nd Aerospace Sciences Meeting, Reno, Nevada, January 1994.

[4] J. J. Alonso, L. Martinelli, and A. Jameson. Multigrid unsteady Navier-Stokes calculations with aeroelastic applications. *AIAA paper 95-0048*, AIAA 33rd Aerospace Sciences Meeting, Reno, Nevada, January 1995.

[5] B.K. Anderson, J.L. Thomas, and B. Van Leer. A comparison of flux vector splittings for the Euler equations. AIAA Paper 85-0122, Reno, NV, January 1985.

[6] W.K. Anderson, J.L. Thomas, and D.L. Whitfield. Multigrid acceleration of the flux split Euler equations. AIAA Paper 86-0274, AIAA 24th Aerospace Sciences Meeting, Reno, January 1986.

[7] T.J. Baker. Mesh generation by a sequence of transformations. *Appl. Num. Math.*, 2:515–528, 1986.

[8] N. Balakrishnan and S. M. Deshpande. New upwind schemes with wave-particle splitting for inviscid compressible flows. *Report 91 FM 12*, Indian Institute of Science, 1991.

[9] B. Baldwin and H. Lomax. Thin layer approximation and algebraic model for separated turbulent flow. AIAA Paper 78-257, 1978.

[10] B.S. Baldwin and T.J. Barth. A one-equation turbulence transport model for high Reynolds number wall-bounded flows. AIAA Paper 91-0610, AIAA 29th Aerospace Sciences Meeting, Reno, NV, January 1991.

[11] T. J. Barth. Aspects of unstructured grids and finite volume solvers for the Euler and Navier Stokes equations. In *von Karman Institute for Fluid Dynamics Lecture Series Notes 1994-05*, Brussels, 1994.

[12] T.J. Barth and P.O. Frederickson. Higher order solution of the Euler equations on unstructured grids using quadratic reconstruction. AIAA paper 90-0013, January 1990.

[13] T.J. Barth and D.C. Jespersen. The design and application of upwind schemes on unstructured meshes. *AIAA paper 89-0366*, AIAA 27th Aerospace Sciences Meeting, Reno, Nevada, January 1989.

[14] J.T. Batina. Implicit flux-split Euler schemes for unsteady aerodynamic analysis involving unstructured dynamic meshes. AIAA paper 90-0936, April 1990.

[15] F. Bauer, P. Garabedian, D. Korn, and A. Jameson. *Supercritical Wing Sections II.* Springer Verlag, New York, 1975.

[16] O. Baysal and M. E. Eleshaky. Aerodynamic design optimization using sensitivity anaysis and computational fluid dynamics. *AIAA paper 91-0471*, 29th Aerospace Sciences Meeting, Reno, Nevada, January 1991.

[17] R.W. Beam and R.F. Warming. An implicit finite difference algorithm for hyperbolic systems in conservation form. *J. Comp. Phys.*, 23:87–110, 1976.

[18] A. Belov, L. Martinelli, and A. Jameson. A new implicit algorithm with multigrid for unsteady incompressible flow calculations. *AIAA paper 95-0049*, AIAA 33rd Aerospace Sciences Meeting, Reno, Nevada, January 1995.

[19] J.A. Benek, P.G. Buning, and J.L. Steger. A 3-D Chimera grid embedding technique. In *Proceedings AIAA 7th Computational Fluid Dynamics Conference*, pages 507–512, Cincinnati, OH, 1985. AIAA Paper 85-1523.

[20] J.A. Benek, T.L. Donegan, and N.E. Suhs. Extended Chimera grid embedding scheme with applications to viscous flows. AIAA Paper 87-1126, AIAA 8th Computational Fluid Dynamics Conference, Honolulu, HI, 1987.

[21] M. Berger and A. Jameson. Automatic adaptive grid refinement for the Euler equations. *AIAA Journal*, 23:561–568, 1985.

[22] M. Berger and R.J. LeVeque. An adaptive Cartesian mesh algorithm for the Euler equations in arbitrary geometries. AIAA Paper 89-1930, 1989.

[23] J.P. Boris and D.L. Book. Flux corrected transport, 1 SHASTA, a fluid transport algorithm that works. *J. Comp. Phys.*, 11:38–69, 1973.

[24] A. Brandt. Multi-level adaptive solutions to boundary value problems. *Math. Comp.*, 31:333–390, 1977.

[25] M.O. Bristeau, R. Glowinski, J. Periaux, P. Perrier, O. Pironneau, and C. Poirier. On the numerical solution of nonlinear problems in fluid dynamics by least squares and finite element methods (II), application to transonic flow simulations. *Comp. Meth. Appl. Mech. and Eng.*, 51:363–394, 1985.

[26] R.J. Busch, Jr. Computational fluid dynamics in the design of the Northrop/McDonnell Douglas YF-23 ATF prototype. *AIAA paper 91-1627*, AIAA 21st Fluid Dynamics, Plasmadynamics & Lasers Conference, Honolulu, Hawaii, 1991.

[27] C. Canuto, M.Y. Hussaini, A. Quarteroni, and D.A. Zang. *Spectral Methods in Fluid Dynamics.* Springer Verlag, 1987.

[28] M.H. Carpenter, D. Gottlieb, and S. Abarbanel. Time-stable boundary conditions for finite-difference schemes solving hyperbolic systems: Methodology and application to high-order compact schemes. ICASE Report 93-9, Hampton, VA, March 1993.

[29] D.A. Caughey. A diagonal implicit multigrid algorithm for the Euler equations. AIAA Paper 87-453, 25th Aerospace Sciences Meeting, Reno, January 1987.

[30] T. Cebeci and A.M.O. Smith. *Analysis of Turbulent Boundary Layers.* Academic Press, 1974.

[31] S.R. Chakravarthy. Relaxation methods for unfactored implicit upwind schemes. AIAA Paper 84-0165, AIAA 22nd Aerospace Sciences Meeting, Reno, January 1984.

[32] S.R. Chakravarthy, A. Harten, and S. Osher. Essentially non-oscillatory shock capturing schemes of uniformly very high accuracy. AIAA Paper 86-0339, AIAA 24th Aerospace Sciences Meeting, Reno, January 1986.

[33] R. Chipman and A. Jameson. Fully conservative numerical solutions for unsteady irrotational transonic flow about airfoils. AIAA Paper 79-1555, AIAA 12th Fluid and Plasma Dynamics Conference, Williamsburg, VA, July 1979.

[34] S.E. Cliff and S.D. Thomas. Euler/experimental correlations of sonic boom pressure signatures. AIAA Paper 91-3276, AIAA 9th Applied Aerodynamics Conference, Baltimore, September 1991.

[35] T.J. Coakley. Numerical simulation of viscous transonic airfoil flows. AIAA Paper 87-0416, AIAA 25th Aerospace Sciences Meeting, Reno, January 1987.

[36] J.P. Croisille and P. Villedieu. Kinetic flux splitting schemes for hypersonic flows. In M. Napolitano and F. Sobetta, editors, *Proc 13th International Congress on Numerical Methods in Fluid Dynamics*, pages 310–313, Rome, July 1992. Springer Verlag.

[37] R.M. Cummings, Y.M. Rizk, L.B. Schiff, and N.M. Chaderjian. Navier-Stokes predictions for the F-18 wing and fuselage at large incidence. *J. of Aircraft*, 29:565–574, 1992.

[38] G. Dahlquist. A special stability problem for linear multistep methods. *BIT*, 3:27–43, 1963.

[39] J.F. Dannenhoffer and J.R. Baron. Robust grid adaptation for complex transonic flows. AIAA Paper 86-0495, AIAA 24th Aerospace Sciences Meeting, Reno, January 1986.

[40] D. Deganiand and L. Schiff. Computation of turbulent supersonic flows around pointed bodies having crossflow separation. *J. Comp. Phys.*, 66:173–196, 1986.

[41] B. Delaunay. Sur la sphère vide. *Bull. Acad. Science USSR VII: Class Scil, Mat. Nat.*, pages 793–800, 1934.

[42] S.M. Deshpande. On the Maxwellian distribution, symmetric form and entropy conservation for the Euler equations. NASA TP 2583, 1986.

[43] A. Eberle. A finite volume method for calculating transonic potential flow around wings from the minimum pressure integral. NASA TM 75324, 1978. Translated from MBB UFE 1407(0).

[44] P.R. Eiseman. A multi-surface method of coordinate generation. *J. Comp. Phys.*, 33:118–150, 1979.

[45] W. Eppard and B. Grossman. A multidimensional kinetic-based upwind solver for the Euler equations. AIAA Paper 93-3303, AIAA 11th Computational Fluid Dynamics Conference, Orlando, FL, July 1993.

[46] L.E. Eriksson. Generation of boundary-conforming grids around wing-body configurations using transfinite interpolation. *AIAA Journal*, 20:1313–1320, 1982.

[47] J. Farmer, L. Martinelli, A. Jameson, and G. Cowles. Fully-nonlinear CFD techniques for ship performance analysis and design. *AIAA paper 95-1690*, AIAA 12th Computational Fluid Dynamics Conference, San Diego, CA, June 1995.

[48] R.P. Fedorenko. The speed of convergence of one iterative process. *USSR Comp. Math. and Math. Phys.*, 4:227–235, 1964.

[49] C.W. Gear. The numerical integration of stiff ordinary differential equations. Report 221, University of Illinois Department of Computer Science, 1967.

[50] M. Giles, M. Drela, and W.T. Thompkins. Newton solution of direct and inverse transonic Euler equations. AIAA Paper 85-1530, Cincinnati, 1985.

[51] S.K. Godunov. A difference method for the numerical calculation of discontinuous solutions of hydrodynamic equations. *Mat. Sbornik*, 47:271–306, 1959. Translated as JPRS 7225 by U.S. Dept. of Commerce, 1960.

[52] M.H. Ha. The impact of turbulence modelling on the numerical prediction of flows. In M. Napolitano and F. Solbetta, editors, *Proc. of the 13th International Conference on Numerical Methods in Fluid Dynamics*, pages 27–46, Rome, Italy, July 1992. Springer Verlag, 1993.

[53] W. Hackbusch. On the multi-grid method applied to difference equations. *Computing*, 20:291–306, 1978.

[54] M. Hafez, J.C. South, and E.M. Murman. Artificial compressibility method for numerical solutions of the transonic full potential equation. *AIAA Journal*, 17:838–844, 1979.

[55] M.G. Hall. Cell vertex multigrid schemes for solution of the Euler equations. In *Proc. IMA Conference on Numerical Methods for Fluid Dynamics*, Reading, April 1985.

[56] A. Harten. High resolution schemes for hyperbolic conservation laws. *J. Comp. Phys.*, 49:357–393, 1983.

[57] P.W. Hemker and S.P. Spekreijse. Multigrid solution of the steady Euler equations. In *Proc. Oberwolfach Meeting on Multigrid Methods*, December 1984.

[58] J.L. Hess and A.M.O. Smith. Calculation of non-lifting potential flow about arbitrary three-dimensional bodies. Douglas Aircraft Report ES 40622, 1962.

[59] C. Hirsch, C. Lacol, and H. Deconinck. Convection algorithms based on a diagonalization procedure for the multi-dimensional Euler equations. In *Proc. AIAA 8th Computational Fluid Dynamics Conference*, pages 667–676, Hawaii, June 1987. AIAA Paper 87-1163.

[60] C. Hirsch and P. Van Ransbeeck. Multidimensional upwinding and artificial dissipation. Technical report. Published in *Frontiers of Computational Fluid Dynamics 1994*, D. A. Caughey and M. M. Hafez, editors, Wiley, pp. 597–626.

[61] D.G. Holmes and S.H. Lamson. Adaptive triangular meshes for compressible flow solutions. In *Proceedings First International Conference on Numerical Grid Generation in Computational Fluid Dynamics*, pages 413–424, Landshut, FRG, July 1986.

[62] T.J.R. Hughes, L.P. Franca, and M. Mallet. A new finite element formulation for computational fluid dynamics,I, Symmetric forms of the compressible Euler and Navier-Stokes equations and the second law of thermodynamics. *Comp. Meth. Appl. Mech. and Eng.*, 59:223–231, 1986.

[63] A. Jameson. Iterative solution of transonic flows over airfoils and wings, including flows at Mach 1. *Comm. on Pure and Appl. Math.*, 27:283–309, 1974.

[64] A. Jameson. Transonic potential flow calculations in conservation form. In *Proc. AIAA 2nd Computational Fluid Dynamics Conference*, pages 148–161, Hartford, 1975.

[65] A. Jameson. Solution of the Euler equations by a multigrid method. *Appl. Math. and Comp.*, 13:327–356, 1983.

[66] A. Jameson. Solution of the Euler equations for two dimensional transonic flow by a multigrid method. *Appl. Math. Comp.*, 13:327–356, 1983.

[67] A. Jameson. Multigrid algorithms for compressible flow calculations. In *Second European Conference on Multigrid Methods*, Cologne, October 1985. Princeton University Report MAE 1743.

[68] A. Jameson. Non-oscillatory shock capturing scheme using flux limited dissipation. In B.E. Engquist, S. Osher, and R.C.J. Sommerville, editors, *Lectures in Applied Mathematics, Vol. 22, Part 1, Large Scale Computations in Fluid Mechanics*, pages 345–370. AMS, 1985.

[69] A. Jameson. Transonic flow calculations for aircraft. In F. Brezzi, editor, *Lecture Notes in Mathematics, Numerical Methods in Fluid Dynamics*, pages 156–242. Springer Verlag, 1985.

[70] A. Jameson. Multigrid algorithms for compressible flow calculations. In W. Hackbusch and U. Trottenberg, editors, *Lecture Notes in Mathematics, Vol. 1228*, pages 166–201. Proceedings of the 2nd European Conference on Multigrid Methods, Cologne, 1985, Springer-Verlag, 1986.

[71] A. Jameson. A vertex based multigrid algorithm for three-dimensional compressible flow calculations. In T.E. Tezduar and T.J.R. Hughes, editors, *Numerical Methods for Compressible Flow - Finite Difference, Element And Volume Techniques*, 1986. ASME Publication AMD 78.

[72] A. Jameson. Aerodynamic design via control theory. *J. Sci. Comp.*, 3:233–260, 1988.

[73] A. Jameson. Automatic design of transonic airfoils to reduce the shock induced pressure drag. In *Proceedings of the 31st Israel Annual Conference on Aviation and Aeronautics, Tel Aviv*, pages 5–17, February 1990.

[74] A. Jameson. Time dependent calculations using multigrid, with applications to unsteady flows past airfoils and wings. *AIAA paper 91-1596*, AIAA 10th Computational Fluid Dynamics Conference, Honolulu, Hawaii, June 1991.

[75] A. Jameson. Artificial diffusion, upwind biasing, limiters and their effect on accuracy and multigrid convergence in transonic and hypersonic flows. AIAA Paper 93-3359, AIAA 11th Computational Fluid Dynamics Conference, Orlando, FL, July 1993.

[76] A. Jameson. Artificial diffusion, upwind biasing, limiters and their effect on accuracy and multigrid convergence in transonic and hypersonic flow. *AIAA paper 93-3359*, AIAA 11th Computational Fluid Dynamics Conference, Orlando, Florida, July 1993.

[77] A. Jameson. Optimum aerodynamic design via boundary control. Technical report, AGARD FDP/Von Karman Institute Special Course on Optimum Design Methods in Aerodynamics, Brussels, April 1994.

[78] A. Jameson. MAE Technical Report 2050, Princeton University, Princeton, New Jersey, October 1995.

[79] A. Jameson. Analysis and design of numerical schemes for gas dynamics 1, artificial diffusion, upwind biasing, limiters and their effect on multigrid convergence. *Int. J. of Comp. Fluid Dyn.*, 4:171–218, 1995.

[80] A. Jameson. Analysis and design of numerical schemes for gas dynamics 2, artificial diffusion and discrete shock structure. *Int. J. of Comp. Fluid Dyn.*, To Appear.

[81] A. Jameson and T.J. Baker. Improvements to the aircraft Euler method. AIAA Paper 87-0452, AIAA 25th Aerospace Sciences Meeting, Reno, January 1987.

[82] A. Jameson, T.J. Baker, and N.P. Weatherill. Calculation of inviscid transonic flow over a complete aircraft. AIAA Paper 86-0103, AIAA 24th Aerospace Sciences Meeting, Reno, January 1986.

[83] A. Jameson and D.J. Mavriplis. Multigrid solution of the Euler equations on unstructured and adaptive grids. In S. McCormick, editor, *Multigrid Methods, Theory, Applications and Supercomputing. Lecture Notes in Pure and Applied Mathematics*, volume 110, pages 413–430, April 1987.

[84] A. Jameson, W. Schmidt, and E. Turkel. Numerical solution of the Euler equations by finite volume methods using Runge-Kutta time stepping schemes. AIAA Paper 81-1259, 1981.

[85] A. Jameson, W. Schmidt, and E. Turkel. Numerical solutions of the Euler equations by finite volume methods with Runge-Kutta time stepping schemes. *AIAA paper 81-1259*, January 1981.

[86] A. Jameson and E. Turkel. Implicit schemes and LU decompositions. *Math. Comp.*, 37:385–397, 1981.

[87] M. Jayaram and A. Jameson. Multigrid solution of the Navier-Stokes equations for flow over wings. *AIAA paper 88-0705*, AIAA 26th Aerospace Sciences Meeting, Reno, Nevada, January 1988.

[88] D. Johnson and L. King. A mathematically simple turbulence closure model for attached and separated turbulent boundary layers. *AIAA Journal*, 23:1684–1692, 1985.

[89] W.P. Jones and B.E. Launder. The calculation of low-Reynolds-number phenomena with a two-equation model of turbulence. *Int. J. of Heat Tran.*, 16:1119–1130, 1973.

[90] W.H. Jou. Boeing Memorandum AERO-B113B-L92-018, September 1992. To Joseph Shang.

[91] T.J. Kao, T.Y. Su, and N.J. Yu. Navier-Stokes calculations for transport wing-body configurations with nacelles and struts. AIAA Paper 93-2945, AIAA 24th Fluid Dynamics Conference, Orlando, July 1993.

[92] G.E. Karniadakis and S.A. Orszag. Nodes, modes and flow codes. *Physics Today*, pages 34–42, March 1993.

[93] M.H. Lallemand and A. Dervieux. A multigrid finite-element method for solving the two-dimensional Euler equations. In S.F. McCormick, editor, *Proceedings of the Third Copper Mountain Conference on Multigrid Methods, Lecture Notes in Pure and Applied Mathematics*, pages 337–363, Copper Mountain, April 1987.

[94] A.M. Landsberg, J.P. Boris, W. Sandberg, and T.R. Young. Naval ship superstructure design: Complex three-dimensional flows using an efficient, parallel method. *High Performance Computing 1993: Grand Challenges in Computer Simulation*, 1993.

[95] P. D. Lax. Hyperbolic systems of conservation laws. *SIAM Regional Series on Appl. Math.*, II, 1973.

[96] P.D. Lax. Hyperbolic systems of conservation laws and the mathematical theory of shock waves. *SIAM Regional Series on Appl. Math.*, 11, 1973.

[97] P.D. Lax and B. Wendroff. Systems of conservation laws. *Comm. Pure. Appl. Math.*, 13:217–237, l960.

[98] B. Van Leer. Towards the ultimate conservative difference scheme. II. Monotonicity and conservation combined in a second order scheme. *J. Comp. Phys.*, 14:361–370, 1974.

[99] B. Van Leer. Towards the ultimate conservative difference scheme. III upstream-centered finite-difference schemes for ideal compressible flow. *J. Comp. Phys.*, 23:263–275, 1975.

[100] B. Van Leer. Flux vector splitting for the Euler equations. In E. Krause, editor, *Proceedings of the 8th International Conference on Numerical Methods in Fluid Dynamics*, pages 507–512, Aachen, 1982.

[101] B. Van Leer. Progress in multi-dimensional upwind differencing. In M. Napolitano and F. Solbetta, editors, *Proc. 13th International Conference on Numerical Methods in Fluid Dynamics*, pages 1–26, Rome, July 1992. Springer Verlag, 1993.

[102] B. Van Leer, W. T. Lee, and P. L. Roe. Characteristic time stepping or local preconditioning of the Euler equations. *AIAA paper 91-1552*, AIAA 10th Computational Fluid Dynamics Conference, Honolulu, Hawaii, June 1991.

[103] D. Lefebre, J.Peraire, and K.Morgan. Finite element least squares solutions of the Euler equations using linear and quadratic approximations. *Int. J. Comp. Fluid Dynamics*, 1:1–23, 1993.

[104] S.K. Lele. Compact finite difference schemes with spectral-like resolution. CTR Manuscript 107, 1990.

[105] J.L. Lions. *Optimal Control of Systems Governed by Partial Differential Equations*. Springer-Verlag, New York, 1971. Translated by S.K. Mitter.

[106] M-S. Liou and C.J. Steffen. A new flux splitting scheme. *J. Comp. Phys.*, 107:23–39, 1993.

[107] F. Liu and A. Jameson. Multigrid Navier-Stokes calculations for three-dimensional cascades. *AIAA paper 92-0190*, AIAA 30th Aerospace Sciences Meeting, Reno, Nevada, January 1992.

[108] R. Löhner and D. Martin. An implicit linelet-based solver for incompressible flows. AIAA paper 92-0668, AIAA 30th Aerospace Sciences Meeting, Reno, NV, January 1992.

[109] R. Löhner, K. Morgan, and J. Peraire. Improved adaptive refinement strategies for the finite element aerodynamic configurations. AIAA Paper 86-0499, AIAA 24th Aerospace Sciences Meeting, Reno, January 1986.

[110] R. Löhner, K. Morgan, J. Peraire, and O.C. Zienkiewicz. Finite element methods for high speed flows. In *Proc. AIAA 7th Computational Fluid Dynamics Conference*, Cincinnati, OH, 1985. AIAA Paper 85-1531.

[111] R. Löhner and P. Parikh. Generation of three-dimensional unstructured grids by the advancing front method. AIAA Paper 88-0515, Reno, NV, January 1988.

[112] R.W. MacCormack and A.J. Paullay. Computational efficiency achieved by time splitting of finite difference operators. AIAA Paper 72-154, 1972.

[113] A. Majda and S. Osher. Numerical viscosity and the entropy condition. *Comm. on Pure Appl. Math.*, 32:797–838, 1979.

[114] L. Martinelli and A. Jameson. Validation of a multigrid method for the Reynolds averaged equations. *AIAA paper 88-0414*, 1988.

[115] L. Martinelli, A. Jameson, and E. Malfa. Numerical simulation of three-dimensional vortex flows over delta wing configurations. In M. Napolitano and F. Solbetta, editors, *Proc. 13th International Confrence on Numerical Methods in Fluid Dynamics*, pages 534–538, Rome, Italy, July 1992. Springer Verlag, 1993.

[116] L. Martinelli and V. Yakhot. RNG-based turbulence transport approximations with applications to transonic flows. AIAA Paper 89-1950, AIAA 9th Computational Fluid Dynamics Conference, Buffalo, NY, June 1989.

[117] D.J. Mavriplis and A. Jameson. Multigrid solution of the Navier-Stokes equations on triangular meshes. *AIAA Journal*, 28(8):1415–1425, August 1990.

[118] D.J. Mavriplis and L. Martinelli. Multigrid solution of compressible turbulent flow on unstructured meshes using a two-equation model. AIAA Paper 91-0237, January 1991.

[119] N. D. Melson, M. D. Sanetrik, and H. L. Atkins. Time-accurate Navier-Stokes calculations with multigrid acceleration. In *Proceedings of the Sixth Copper Mountain Conference on Multigrid Methods*, Copper Mountain, April 1993.

[120] J.E. Melton, S.A. Pandya, and J.L. Steger. 3D Euler flow solutions using unstructured Cartesian and prismatic grids. AIAA Paper 93-0331, Reno, NV, January 1993.

[121] F. Menter. Zonal two-equation k-ω turbulence models for aerodynamic flows. AIAA Paper 93-2906, AIAA 24th Fluid Dynamics Meeting, Orlando, July 1993.

[122] E.M. Murman. Analysis of embedded shock waves calculated by relaxation methods. *AIAA Journal*, 12:626–633, 1974.

[123] E.M. Murman and J.D. Cole. Calculation of plane steady transonic flows. *AIAA Journal*, 9:114–121, 1971.

[124] R.H. Ni. A multiple grid scheme for solving the Euler equations. *AIAA Journal*, 20:1565–1571, 1982.

[125] S. Obayashi and K. Kuwakara. LU factorization of an implicit scheme for the compressible Navier-Stokes equations. AIAA Paper 84-1670, AIAA 17th Fluid Dynamics and Plasma Dynamics Conference, Snowmass, June 1984.

[126] J.T. Oden, L. Demkowicz, T. Liszka, and W. Rachowicz. *h-p* adaptive finite element methods for compressible and incompressible flows. In S. L. Venneri A. K. Noor, editor, *Proceedings of the Symposium on Computational Technology on Flight Vehicles*, pages 523–534, Washington, D.C., November 1990. Pergamon.

[127] S. Orszag and D. Gottlieb. Numerical analysis of spectral methods. *SIAM Regional Series on Appl. Math.*, 26, 1977.

[128] S. Osher. Riemann solvers, the entropy condition, and difference approximations. *SIAM J. Num. Anal.*, 121:217–235, 1984.

[129] S. Osher and S. Chakravarthy. High resolution schemes and the entropy condition. *SIAM J. Num Anal.*, 21:955–984, 1984.

[130] S. Osher and F. Solomon. Upwind difference schemes for hyperbolic systems of conservation laws. *Math. Comp.*, 38:339–374, 1982.

[131] S. Osher and E. Tadmor. On the convergence of difference approximations to scalar conservation laws. *Math. Comp.*, 50:19–51, 1988.

[132] H. Paillère and H. Deconinck. A review of multi-dimensional upwind residual distribution schemes for the euler equations. *To appear in CFD Review*, 1995.

[133] N. A. Pierce and M. B. Giles. Preconditioning on stretched meshes. Report 95/10 1995, Oxford University Computing Laboratory, Oxford, December 1995.

[134] O. Pironneau. *Optimal Shape Design for Elliptic Systems*. Springer-Verlag, New York, 1984.

[135] K.G. Powell and B. van Leer. A genuinely multidimensional upwind cell-vertex scheme for the Euler equations. AIAA Paper 89-0095, AIAA 27th Aerospace Sciences Meeting, Reno, January 1989.

[136] K. Prendergast and K. Xu. Numerical hydrodynamics from gas kinetic theory. *J. Comp. Phys.*, 109:53–66, November 1993.

[137] T.H. Pulliam and J.L. Steger. Implicit finite difference simulations of three-dimensional compressible flow. *AIAA Journal*, 18:159–167, 1980.

[138] J.J. Quirk. An alternative to unstructured grids for computing gas dynamics flows about arbitrarily complex two-dimensional bodies. ICASE Report 92-7, Hampton, VA, February 1992.

[139] R. Radespiel, C. Rossow, and R.C. Swanson. An efficient cell-vertex multigrid scheme for the three-dimensional Navier-Stokes equations. In *Proc. AIAA 9th Computational Fluid Dynamics Conference*, pages 249–260, Buffalo, NY, June 1989. AIAA Paper 89-1953-CP.

[140] M.M. Rai and P. Moin. Direct numerical simulation of transition and turbulence in a spatially evolving boundary layer. AIAA Paper 91-1607 CP, AIAA 10th Computational Fluid Dynamics Conference, Honolulu, HI, June 1991.

[141] S. V. Rao and S. M. Deshpande. A class of efficient kinetic upwind methods for compressible flows. *Report 91 FM 11*, Indian Institute of Science, 1991.

[142] J. Reuther and A. Jameson. Aerodynamic shape optimization of wing and wing-body configurations using control theory. *AIAA paper 95-0213*, 33rd Aerospace Sciences Meeting and Exibit, Reno, Nevada, January 1995.

[143] J. Reuther and A. Jameson. Aerodynamic shape optimization of wing and wing-body configurations using control theory. *AIAA paper 95-0123*, AIAA 33rd Aerospace Sciences Meeting, Reno, Nevada, January 1995.

[144] H. Rieger and A. Jameson. Solution of steady three-dimensional compressible Euler and Navier-Stokes equations by and implicit LU scheme. *AIAA paper 88-0619*, AIAA 26th Aerospace Sciences Meeting, Reno, Nevada, January 1988.

[145] A. Rizzi and L.E. Eriksson. Computation of flow around wings based on the Euler equations. *J. Fluid Mech.*, 148:45–71, 1984.

[146] P.L. Roe. Approximate Riemann solvers, parameter vectors, and difference schemes. *J. Comp. Phys.*, 43:357–372, 1981.

[147] P.E. Rubbert and G.R. Saaris. A general three-dimensional potential flow method applied to V/STOL aerodynamics. SAE Paper 680304, 1968.

[148] C.L. Rumsey and V.N. Vatsa. A comparison of the predictive capabilities of several turbulence models using upwind and centered - difference computer codes. AIAA Paper 93-0192, AIAA 31st Aerospace Sciences Meeting, Reno, January 1993.

[149] S.S. Samant, J.E. Bussoletti, F.T. Johnson, R.H. Burkhart, B.L. Everson, R.G. Melvin, D.P. Young, L.L. Erickson, and M.D. Madson. TRANAIR: A computer code for transonic analyses of arbitrary configurations. AIAA Paper 87-0034, 1987.

[150] K. Sawada and S. Takanashi. A numerical investigation on wing/nacelle interferences of USB configuration. In *Proceedings AIAA 25th Aerospace Sciences Meeting*, Reno, NV, 1987. AIAA paper 87-0455.

[151] C.W. Shu and S. Osher. Efficient implementation of essentially non-oscillatory shock-capturing schemes. *J. Comp. Phys.*, 77:439–471, 1988.

[152] C.W. Shu and S. Osher. Efficient implementation of essentially non-oscillatory shock-capturing schemes II. *J. Comp. Phys.*, 83:32–78, 1989.

[153] C.W. Shu, T.A. Zang, G. Erlebacher, D. Whitaker, and S. Osher. High-order ENO schemes applied to two- and three-dimensional compressible flow. *Appl. Num. Math.*, 9:45–71, 1992.

[154] B. R. Smith. A near wall model for the $k-l$ two equation turbulence model. *AIAA paper 94-2386*, 25th AIAA Fluid Dynamics Conference, Colorado Springs, CO, June 1994.

[155] L.M. Smith and W.C. Reynolds. On the Yakhot-Orszag renormalization group for deriving turbulence statistics and models. *Phys. Fluids A*, 4:364–390, 1992.

[156] R.E. Smith. Three-dimensional algebraic mesh generation. In *Proc. AIAA 6th Computational Fluid Dynamics Conference*, Danvers, MA, 1983. AIAA Paper 83-1904.

[157] R.L. Sorenson. Elliptic generation of compressible three-dimensional grids about realistic aircraft. In J. Hauser and C. Taylor, editors, *International Conference on Numerical Grid Generation in Computational Fluid Dynamics*, Landshut, F. R. G., 1986.

[158] R.L. Sorenson. Three-dimensional elliptic grid generation for an F-16. In J.L. Steger and J.F. Thompson, editors, *Three-Dimensional Grid Generation for Complex Configurations: Recent Progress*, 1988. AGARDograph.

[159] P. Spalart and S. Allmaras. A one-equation turbulent model for aerodynamic flows. AIAA Paper 92-0439, AIAA 30th Aerospace Sciences Meeting, Reno, NV, January 1992.

[160] C.G. Speziale, E.C. Anderson, and R. Abid. A critical evaluation of two-equation models for near wall turbulence. AIAA Paper 90-1481, June 1990. ICASE Report 90-46.

[161] J.L. Steger and D.S. Chaussee. Generation of body-fitted coordinates using hyperbolic partial differential equations. *SIAM J. Sci. and Stat. Comp.*, 1:431–437, 1980.

[162] J.L. Steger and R.F. Warming. Flux vector splitting of the inviscid gas dynamic equations with applications to finite difference methods. *J. Comp. Phys.*, 40:263–293, 1981.

[163] B. Stoufflet, J. Periaux, F. Fezoui, and A. Dervieux. Numerical simulation of 3-D hypersonic Euler flows around space vehicles using adapted finite elements. AIAA paper 87-0560, January 1987.

[164] R.C. Swanson and E. Turkel. On central-difference and upwind schemes. *J. Comp. Phys.*, 101:297–306, 1992.

[165] P.K. Sweby. High resolution schemes using flux limiters for hyperbolic conservation laws. *SIAM J. Num. Anal.*, 21:995–1011, 1984.

[166] S. Ta'asan, G. Kuruvila, and M. D. Salas. Aerodynamic design and optimization in one shot. *AIAA paper 92-005*, 30th Aerospace Sciences Meeting and Exibit, Reno, Nevada, January 1992.

[167] Shlomo Ta'asan. Canonical forms of multidimensional, steady inviscid flows. ICASE 93-34, Institute for Computer Applications in Science and Engineering, Hampton, VA, 1993.

[168] E. Tadmor. Numerical viscosity and the entropy condition for conservative difference schemes. *Math. Comp.*, 32:369–382, 1984.

[169] J.F. Thompson, F.C. Thames, and C.W. Mastin. Automatic numerical generation of body-fitted curvilinear coordinate system for field containing any number of arbitrary two-dimensional bodies. *J. Comp. Phys.*, 15:299–319, 1974.

[170] J.F. Thompson, Z.U.A. Warsi, and C.W. Mastin. Boundary-fitted coordinate systems for numerical solution of partial differential equations: A review. *J. Comp. Phys.*, 47:1–108, 1982.

[171] E. Turkel. Preconditioned methods for solving the incompressible and low speed equations. *J. Comp. Phys.*, 72:277–298, 1987.

[172] V. Venkatakrishnan. Newton solution of inviscid and viscous problems. AIAA paper 88-0413, January 1988.

[173] V. Venkatakrishnan. Convergence to steady state solutions of the Euler equations on unstructured grids with limiters. *AIAA paper 93-0880*, AIAA 31st Aerospace Sciences Meeting, Reno, Nevada, January 1993.

[174] G. Voronoï. Nouvelles applications des parametres continus à la théorie des formes quadratiques. Deuxième mémoire: Recherches sur les parallelloedres primitifs. *J. Reine Angew. Math.*, 134:198–287, 1908.

[175] Y. Wada and M-S. Liou. A flux splitting scheme with high-resolution and robustness for discontinuities. *AIAA paper 94-0083*, AIAA 32nd Aerospace Sciences Meeting, Reno, Nevada, January 1994.

[176] N.P. Weatherill and C.A. Forsey. Grid generation and flow calculations for aircraft geometries. *J. Aircraft*, 22:855–860, 1985.

[177] D.C. Wilcox. A half a century historical review of the k-ω model. AIAA Paper 91-0615, AIAA 29th Aerospace Sciences Meeting, Reno, NV, January 1991.

[178] F. Woodward. An improved method for the aerodynamic analysis of wing-body-tail configurations in subsonic and supersonic flow, Part 1 — theory and application. NASA CR 2228 Pt. 1, May 1973.

[179] P. Woodward and P. Colella. The numerical simulation of two-dimensional fluid flow with strong shocks. *J. Comp. Phys.*, 54:115–173, 1984.

[180] K. Xu, L. Martinelli, and A. Jameson. Gas-kinetic finite volume methods, flux-vector splitting and artificial diffusion. *J. Comp. Phys.*, 120:48–65, 1995.

[181] V. Yakhot and S.A. Orszag. Renormalization group analysis of turbulence. I. Basic theory. *J. Sci. Comp.*, 1:3–51, 1986.

[182] H.C. Yee. On symmetric and upwind TVD schemes. In *Proc. 6th GAMM Conference on Numerical Methods in Fluid Mechanics*, Gottingen, September 1985.

[183] S. Yoon and A. Jameson. Lower-upper Symmetric-Gauss-Seidel method for the Euler and Navier-Stokes equations. AIAA Paper 87-0600, AIAA 25th Aerospace Sciences Meeting, Reno, January 1987.

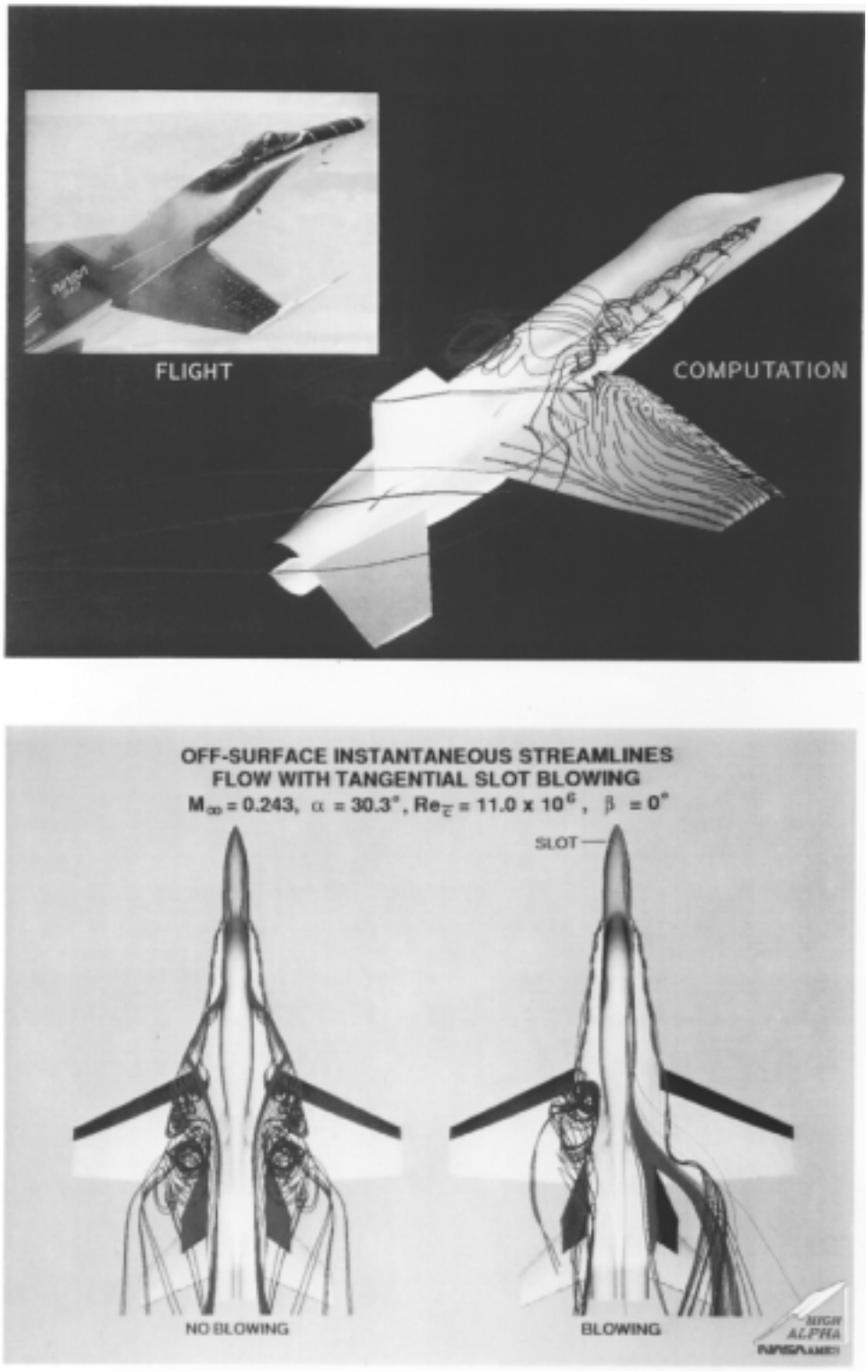

Figure 18: Navier-Stokes Predictions for the F-18 Wing-Fuselage at Large Incidence

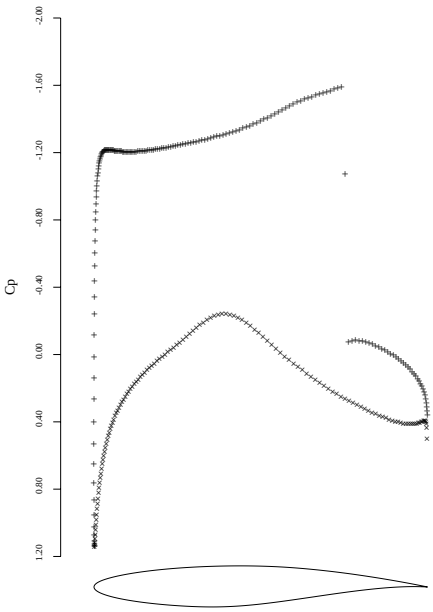

19a: C_p after 25 Cycles.
$C_l = 1.1312$, $C_d = 0.0469$.

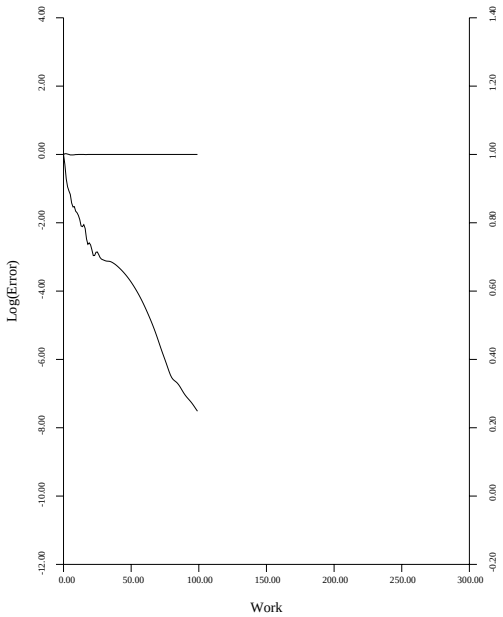

19b: Convergence.

Figure 19: RAE-2822 Airfoil at Mach 0.750 and $\alpha = 3.0°$H-CUSP Scheme.

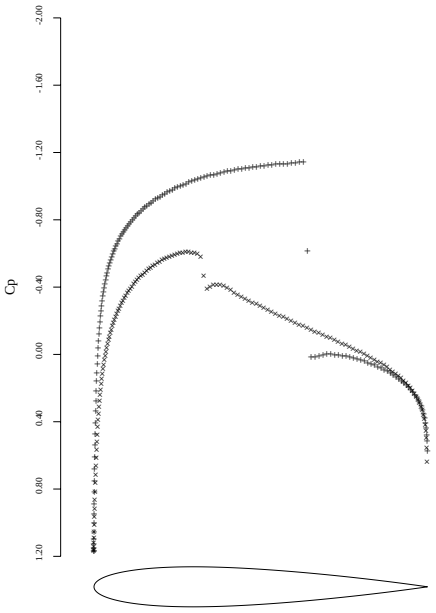

20a: C_p after 35 Cycles.
$C_l = 0.3654$, $C_d = 0.0232$.

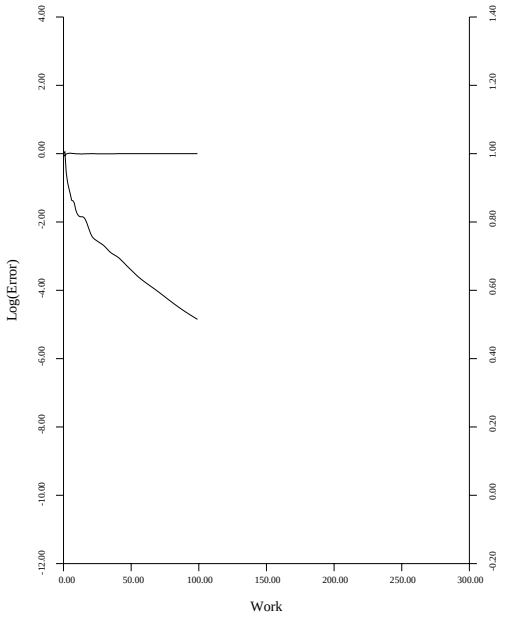

20b: Convergence.

Figure 20: NACA-0012 Airfoil at Mach 0.800 and $\alpha = 1.25°$H-CUSP Scheme.

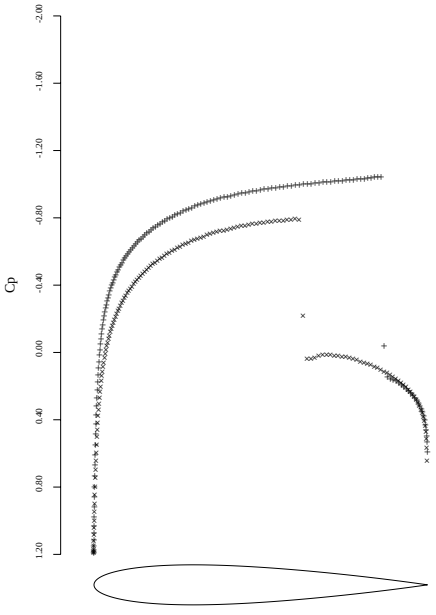

21a: C_p after 35 Cycles.
$C_l = 0.3861$, $C_d = 0.0582$.

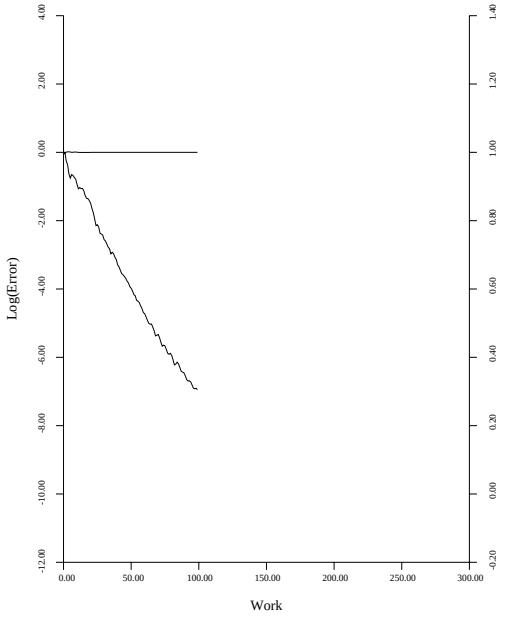

21b: Convergence.

Figure 21: NACA-0012 Airfoil at Mach 0.850 and $\alpha = 1.0°$H-CUSP Scheme.

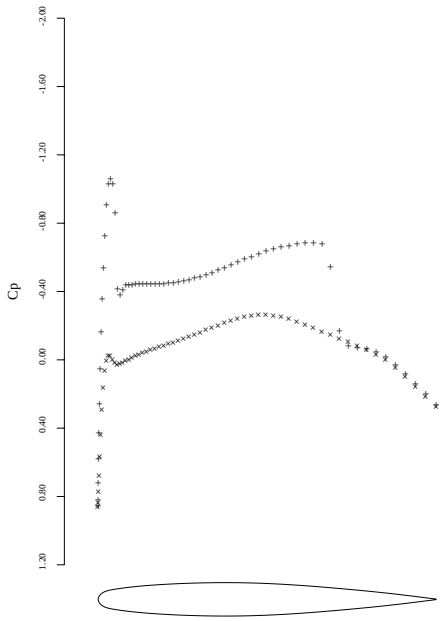

22a: 12.50% Span.
$C_l = 0.2933$, $C_d = 0.0274$.

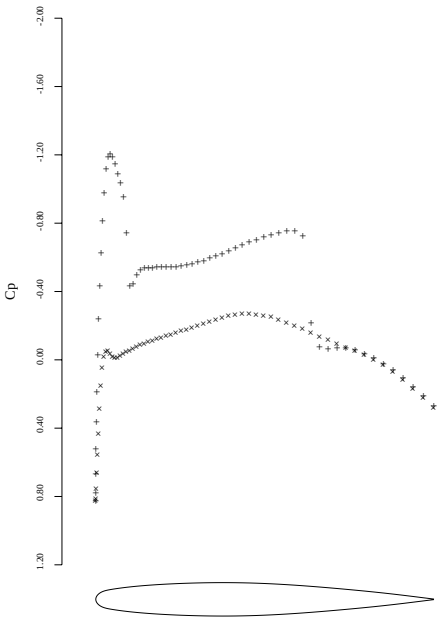

22b: 31.25% Span.
$C_l = 0.3139$, $C_d = 0.0159$.

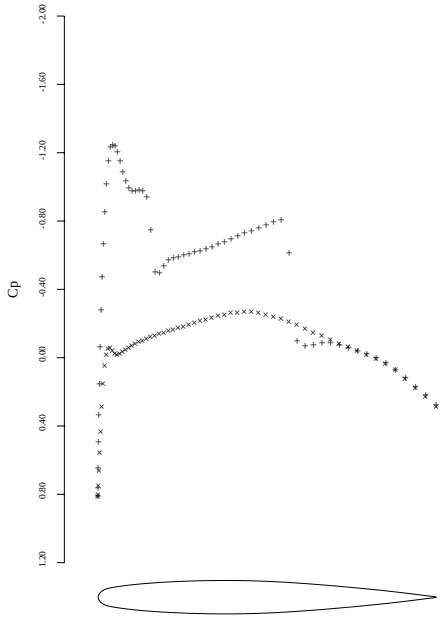

22c: 50.00% Span.
$C_l = 0.3262$, $C_d = 0.0089$.

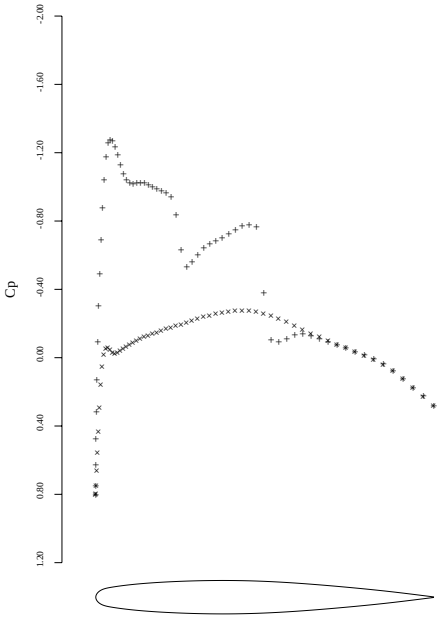

22d: 68.75% Span.
$C_l = 0.3195$, $C_d = 0.0026$.

Figure 22: Onera M6 Wing. Mach 0.840, Angle of Attack 3.06°, 192×32×48 Mesh. $C_L = 0.3041$, $C_D = 0.0131$. H-CUSP scheme.

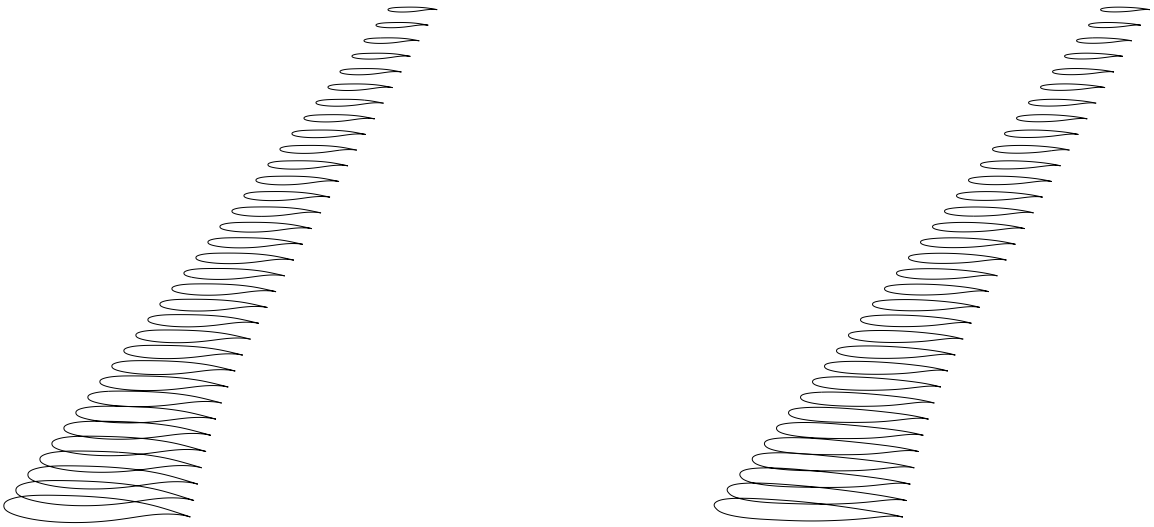

23a: Initial Wing
$C_L = 0.5001$, $C_D = 0.0210$, $\alpha = -1.672°$

23b: 40 Design Iterations
$C_L = 0.5000$, $C_D = 0.0112$, $\alpha = -0.283°$

Figure 23: Swept Wing Design Case (1), $M = 0.85$, Fixed Lift Mode.Drag Reduction at $C_L = .5$.

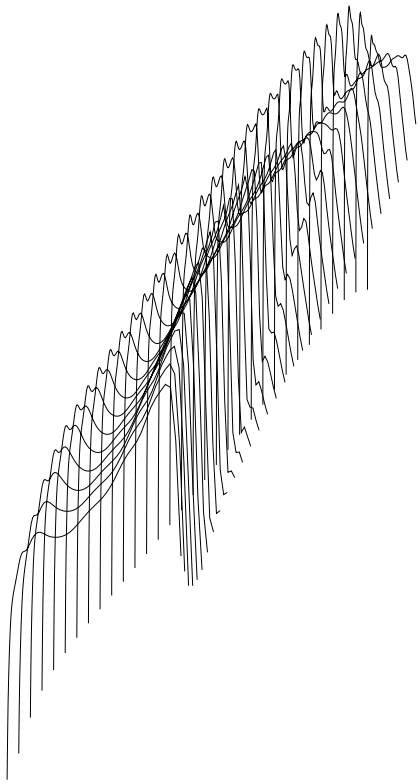

UPPER SURFACE PRESSURE

24a: Initial Wing
$C_L = 0.5001$, $C_D = 0.0210$, $\alpha = -1.672°$

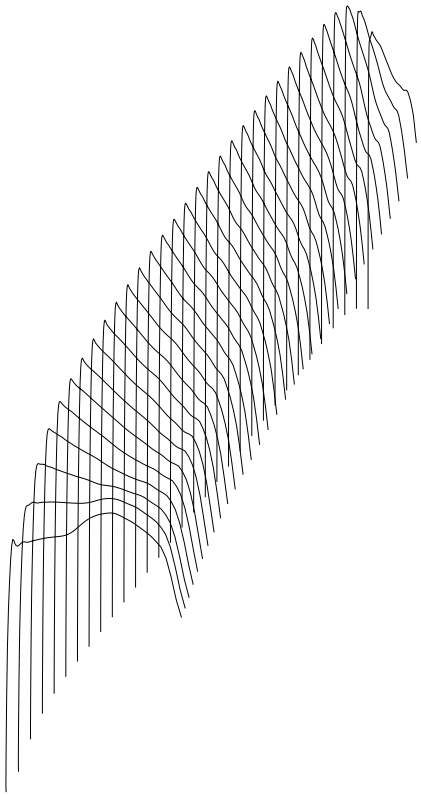

UPPER SURFACE PRESSURE

24b: 40 Design Iterations
$C_L = 0.5000$, $C_D = 0.0112$, $\alpha = -0.283°$

Figure 24: Swept Wing Design Case (1), $M = 0.85$, Fixed Lift Mode.Drag Reduction at $C_L = 0.50$

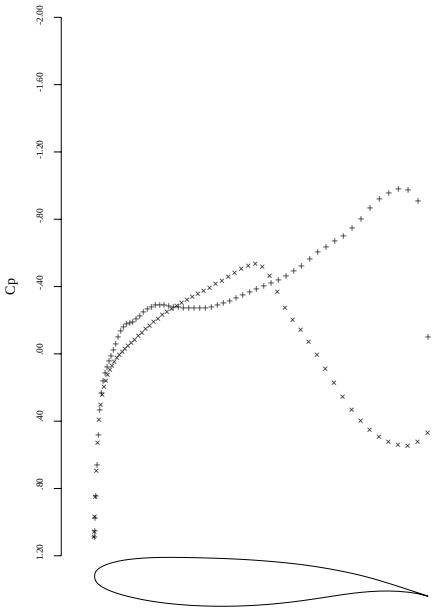

25a: span station $z = 0.00$

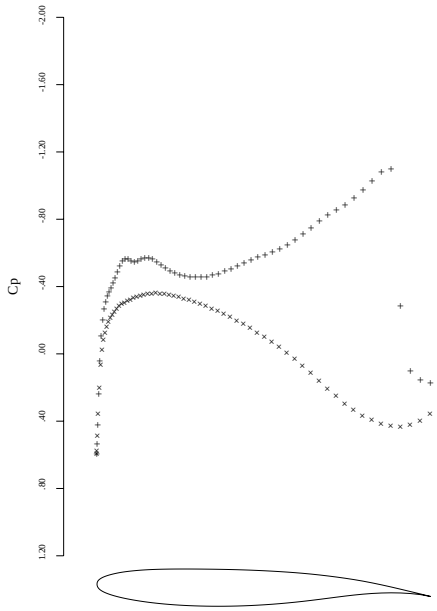

25b: span station $z = 0.312$

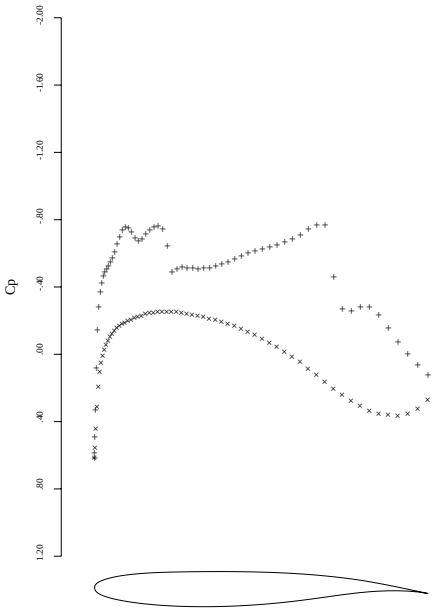

25c: span station $z = 0.625$

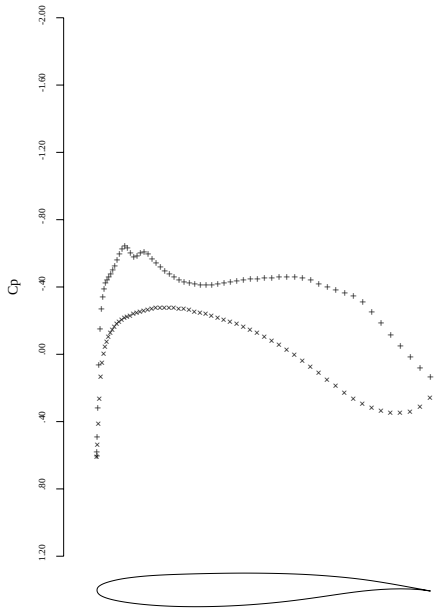

25d: span station $z = 0.937$

Figure 25: FLO67 solution for initial wing.$M = 0.85$, $C_L = 0.4997$, $C_D = 0.0207$, $\alpha = -1.970°$.

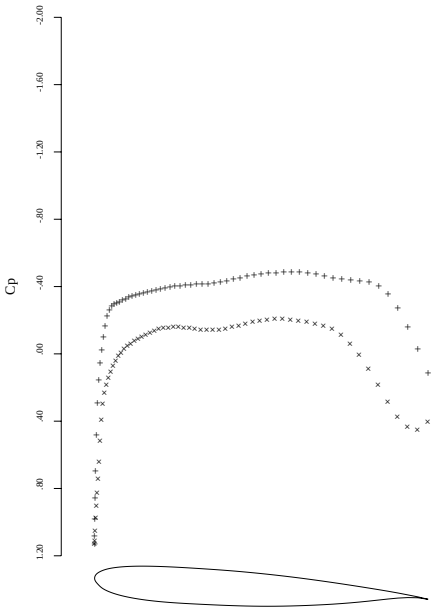

26a: span station $z = 0.00$

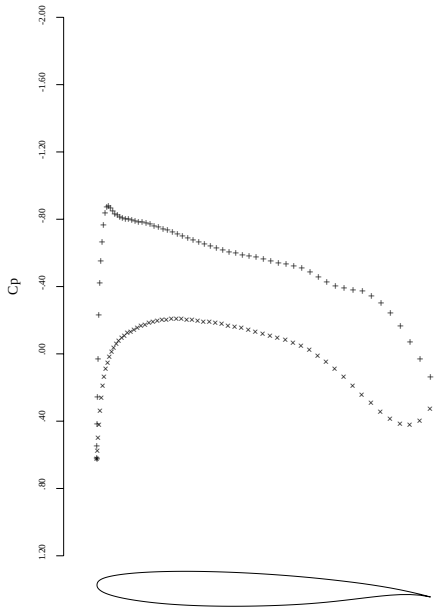

26b: span station $z = 0.312$

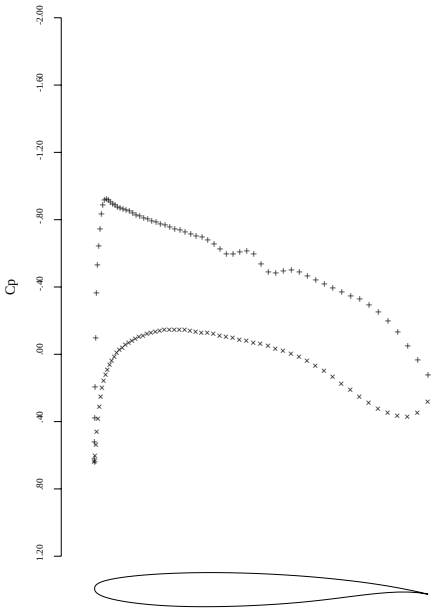

26c: span station $z = 0.625$

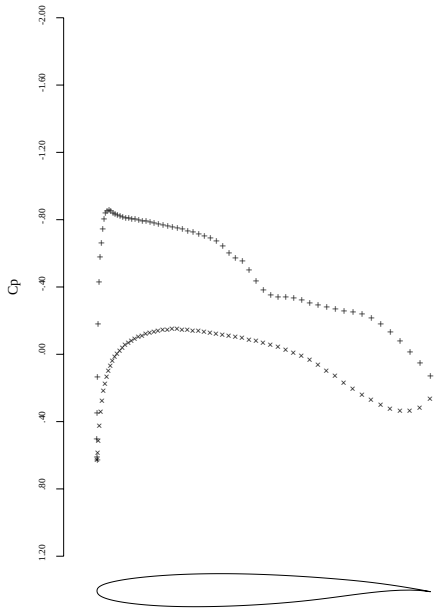

26d: span station $z = 0.937$

Figure 26: FLO67 check on redesigned wing.$M = 0.85$, $C_L = 0.4992$, $C_D = 0.0094$, $\alpha = -0.300°$.

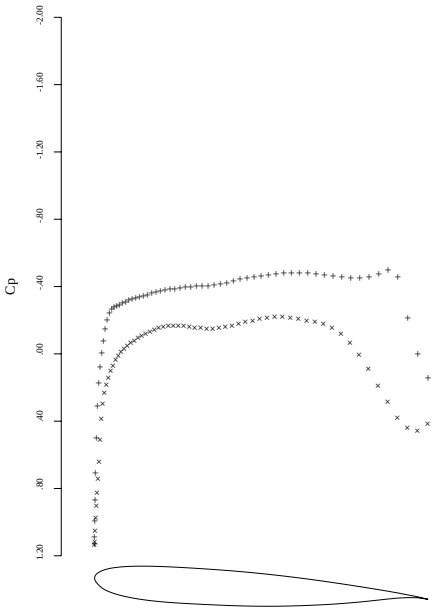

27a: span station $z = 0.00$

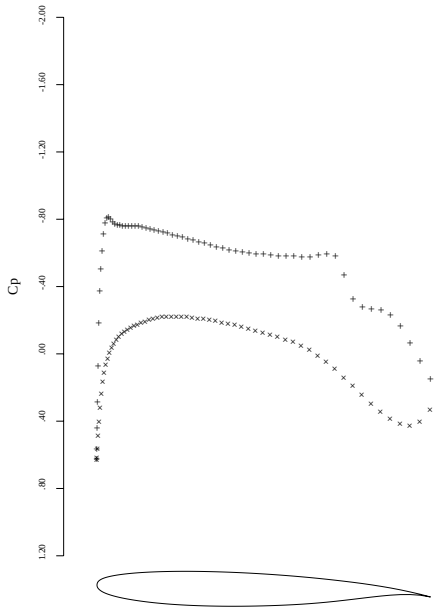

27b: span station $z = 0.312$

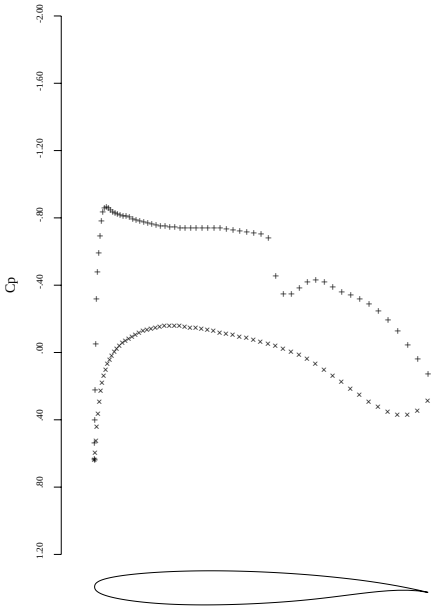

27c: span station $z = 0.625$

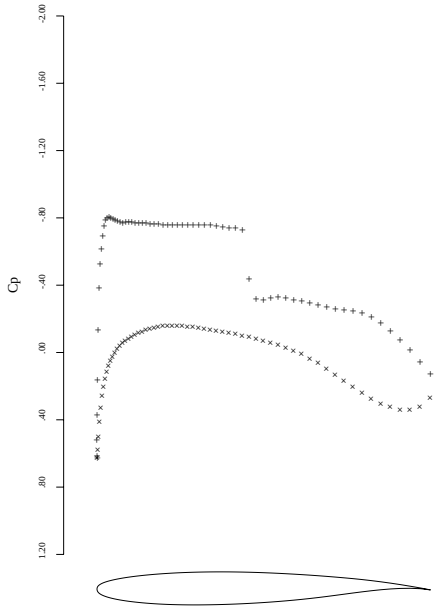

27d: span station $z = 0.937$

Figure 27: FLO67 check on redesigned wing at a higher Mach number. $M = 0.86$, $C_L = 0.4988$, $C_D = 0.0097$, $\alpha = -0.440°$.